Symmetry breaking in vortex-source and Jeffery–Hamel flows

By M. GOLDSHTIK†, F. HUSSAIN AND V. SHTERN†

Department of Mechanical Engineering, University of Houston, Houston,
TX 77204-7492, USA

The stability and bifurcations associated with the loss of azimuthal symmetry of planar flows of a viscous incompressible fluid, such as vortex-source and Jeffery–Hamel flows, are studied by employing linear, weakly nonlinear and fully nonlinear analyses, and features of new solutions are explained. We address here steady self-similar solutions of the Navier–Stokes equations and their stability to spatially developing disturbances. By considering bifurcations of a potential vortex-source flow, we find secondary solutions. They include asymmetric vortices which are generalizations of the classical point vortex to vortical flows with non-axisymmetric vorticity distributions. Another class of solutions we report relates to transition trajectories that connect new bifurcation-produced solutions with the primary ones. Such solutions provide far-field asymptotes for a number of jet-like flows. In particular, we consider a flow which is a combination of a jet and a sink, a tripolar jet, a jet emerging from a slit in a plane wall, a jet emerging from a plane channel and the reattachment phenomenon in the Jeffery–Hamel flow in divergent channels.

CONTENTS

† Permanent address: Institute of Thermophysics, Novosibirsk 630090, USSR.

1. Introduction

This paper addresses stability and bifurcations of elementary hydrodynamic flows such as a point sink, a point source, a point vortex and some of their superpositions and generalizations. We limit our study to plane steady motions of a viscous incompressible fluid. These topics are clearly of intrinsic fundamental hydrodynamic interest, but should also be considered in a much wider context. Such elementary solutions may serve locally as idealized models of convergent, divergent and swirling motions, which are prevalent in natural and technological flows. One encounters such flows as protypical flow modules as well as structural elements in turbulent motions (Hussain 1986) and particularly in jet-like flows.

The main results reported here concern loss of axial symmetry of the above-mentioned primary or base flows and generation of angle-dependent flow patterns as a result of instability. There is a variety of instability mechanisms in jet-like flows: for instance, the well-known free-shear-layer instability (Kelvin–Helmholtz instability), axial symmetry breaking due to spiral mode instability (Batchelor & Gill 1962) and inviscid vortex ring instability (Widnall & Sullivan 1972). In general, theoretical investigation of even linear stability, let alone nonlinear cases, involves numerical calculations and tedious analytical methods. In studies of coherent structure dynamics in turbulent flows and stability of basic flows, we unavoidably

face the question: are the elementary motions themselves subject to instabilities? The principal thrust of this paper is to answer this question. We will also show how simple analytical methods can be used to study linear and nonlinear instabilities of primary flows and bifurcations, as well as asymptotic features of the resulting secondary solutions.

The potential source flow as well as the well-known Jeffery–Hamel (JH) flow belong to a class of (plane) conically similar solutions of the Navier–Stokes equations. The conical flows form a very interesting and intriguing class of solutions of the Navier–Stokes equations (Goldshtik 1990). They possess such unusual effects as collapse of vorticity at finite Reynolds numbers; self-focusing of rotation (Goldshtik & Shtern 1990); and a variety of instabilities which lead, for instance, to self-excitation of swirling and axisymmetric hydromagnetic dynamo. In this paper we deal with *plane* viscous flows only.

Plane conical solutions of the Navier–Stokes equations were first obtained by Jeffery (1915) and Hamel (1916) independently. Following the formulation of the problem by Jeffery, Hamel gave a rather detailed analysis of the flow in a divergent plane channel and found non-uniqueness of steady solutions and non-existence of everywhere-divergent flow regimes at large enough Reynolds numbers. The analysis of spatial stability of the JH solutions seems to have begun with Dean (1934). Rosenhead (1940) found, in addition to other new results, the existence of an infinite number of solutions at any fixed Reynolds number and angle between the plane walls. Fraenkel (1962) showed that as the Reynolds number increases symmetric and asymmetric solutions merge at some critical values. Hooper, Duffy & Moffatt (1982) have studied the JH flow numerically and shown the bifurcation to be subcritical in the Reynolds number – pressure coefficient plane.

Since the works of Fraenkel (1962, 1963), the analysis of the JH problem has been considered as the first step toward the study of the flow in a channel with small wall curvature. This flow's stability has been studied by Georgiou & Eagles (1985, see also references therein) with the help of a small-parameter expansion. Detailed analyses of bifurcations and stability of the JH and generalized flows have been carried out by Sobey & Drazin (1986) and Banks, Drazin & Zaturska (1988). In the latter work the Landau amplitude equation has been used for a weakly nonlinear analysis, and one finds very interesting features of spatial stability. Professor Peralta-Fabi, one of the authors of the paper by Uribe *et al.* (1989), has kindly informed us of their results, which are rather similar to those of Hooper *et al.*, but which include an interesting application of the methods of Hamiltonian mechanics to JH flow.

To our surprise, we have failed to find in the available literature any study of the vortex-source flow stability and bifurcation. We have, however, found that the secondary regimes, appearing as a result of bifurcations, belong to a special class of Navier–Stokes equation solutions. The existence of such a class was indeed noted by Oseen (1927). Some preliminary results have been reported by Goldshtik & Shtern (1989), who found bifurcations of new steady solutions for the source flow. But for the vortex-source flow, they used an approximate approach dealing with unsteady secondary solutions. Recognizing the limitations of the latter approach, here we use the same steady analysis but for the general case of the vortex-source flow and, in addition, study linear and nonlinear spatial stability of the primary and secondary solutions, find new scaling and asymptotic features of the solutions, and study a number of transition trajectories of physical significance.

In particular, the transition trajectories give us the far field of a jet emerging from a slit in a plane wall and of a jet emerging from a plane channel. Solutions of

boundary-layer jets, i.e. jets subject to the boundary-layer approximation (see Schlichting 1979 and Loitsyansky 1966 for theoretical treatment), may be applied in a region where the distance from the slit is large in comparison with the slit size, but momentum flux loss due to a jet–wall interaction is negligible. The momentum flux is a unique characteristic of the boundary-layer jet, and the flow rate from the slit is neglected. We know that jets have self-similar solutions only when the exit flow rate is zero (Batchelor 1967, p. 345). For comparison, we consider here jet-like flows with zero flow rate in the far field, without using the boundary-layer approximation. We show that, owing to jet–wall interaction, velocity decays faster than in boundary-layer jets, and we find two regions with different power relations between velocity and radial distance.

2. Problem formulation

We address plane motion of a viscous incompressible fluid. It is convenient to use the vorticity ω and stream-function ψ equations in polar coordinates (r, ϕ) (see Batchelor 1967),

$$\frac{\partial \omega}{\partial t} + v_r \frac{\partial \omega}{\partial r} + v_\phi \frac{\partial \omega}{r\partial \phi} = \nu\left[\frac{1}{r}\frac{\partial}{\partial r}\left(r\frac{\partial \omega}{\partial r}\right) + \frac{1}{r^2}\frac{\partial^2 \omega}{\partial \phi^2}\right];$$

$$\left.\frac{1}{r}\frac{\partial}{\partial r}\left(r\frac{\partial \psi}{\partial r}\right) + \frac{1}{r^2}\frac{\partial^2 \psi}{\partial \phi^2} = \omega; \quad v_r = \frac{1}{r}\frac{\partial \psi}{\partial \phi}; \quad v_\phi = -\frac{\partial \psi}{\partial r}.\right\} \tag{1}$$

A motion driver is assumed to be localized at the origin $(r = 0)$. It may be a point sink, a point source or a point-vortex source. The problem formulation does not include any intrinsic lengthscale. One can see that the appropriate dimensional scaling factor is the kinematic viscosity ν for stream function, νr^{-1} for velocity and νr^{-2} for vorticity. We choose to introduce new independent variables: $\xi = \ln(r/r_0)$ instead of r, where r_0 is an arbitrary lengthscale which is used to make the argument dimensionless, and $T = \frac{1}{2}\ln(\nu t/r^2)$ instead of time t; and dependent variables

$$v_r = \frac{\nu}{r}U(T, \xi, \phi); \quad v_\phi = \frac{\nu}{r}V(T, \xi, \phi); \quad \psi = \nu\Psi(T, \xi, \phi); \quad \omega = \frac{\nu}{r^2}\Omega(T, \xi, \phi).$$

Substituting these representations into (1) we have,

$$\frac{1}{2}e^{-2T}\frac{\partial \Omega}{\partial T} + \frac{\partial \Psi}{\partial \phi}(D-2)\Omega - \frac{\partial \Omega}{\partial \phi}D\Psi = \frac{\partial^2 \Omega}{\partial \phi^2} + (D-2)^2\Omega,$$

$$\left.D^2\Psi + \frac{\partial^2 \Psi}{\partial \phi^2} = \Omega; \quad U = \frac{\partial \Psi}{\partial \phi}; \quad V = -D\Psi; \quad D = \frac{\partial}{\partial \xi} - \frac{\partial}{\partial T}.\right\} \tag{2}$$

In the simplest case, when in (2), $\partial/\partial T = \partial/\partial \xi = 0$, it follows that $V = 0$ and

$$U''' + 4U' + 2UU' = 0, \tag{3}$$

where the prime denotes differentiation with respect to the azimuthal angle ϕ. After integration this equation becomes

$$U'' + 4U + U^2 = C, \tag{4}$$

which was first derived by Jeffery (1915) and Hamel (1916); this is the JH flow. The integration constant C is related to the Reynolds number

$$Re = \nu^{-1} \int_0^\alpha r v_r \, \mathrm{d}\phi = \alpha U_0.$$

Here the subscript 0 denotes the average with respect to ϕ. Note that a positive Re denotes a source flow and a negative Re denotes a sink flow. As a characteristic of the JH solutions, we will also use the parameter

$$Ba = \frac{r}{4} \frac{\alpha^2}{\nu} v_{r\,\mathrm{max}},$$

where $v_{r\,\mathrm{max}}$ is the maximum radial velocity at a fixed r.

Let us discuss the boundary conditions. For a divergent channel with plane walls at $\phi = 0$ and $\phi = \alpha$, the non-slip boundary conditions are

$$U = V = 0 \quad \text{at} \quad \phi = 0 \quad \text{and} \quad \phi = \alpha. \tag{5}$$

In free space, $\alpha = 2\pi$ and all functions U, V, Ω must be 2π-periodic with respect to ϕ, but the stream function Ψ may have an additional linear term. In particular, it is evident that equations (2) have the solution

$$\Psi = \Psi_o = U_0 \phi - V_0 \xi; \quad \Omega = 0, \tag{6}$$

which corresponds to a potential vortex-source flow. Here U_0 is a constant related to the dimensionless mean radial velocity $U_0 = Re/(2\pi)$, and V_0 is the mean dimensionless azimuthal velocity, which is proportional to circulation, i.e.

$$V_0 = \frac{1}{2\pi\nu} \int_0^{2\pi} v_\phi r \, \mathrm{d}\phi.$$

So far, we have discussed the boundary conditions for the angular coordinate ϕ. Now, with respect to the radial coordinate, we look for solutions (involving U, V, Ω) which remain bounded as $r \to \infty$; we require that Ψ may not have more than the logarithmic singularity, in accord with Ψ_0 behaviour, which is linear in $\xi = \ln(r/r_0)$.

To seek new solutions differing from the classical ones, we shall use here methods of hydrodynamic stability and bifurcation theory (Yudovich 1965; Joseph 1976). Bifurcation of the asymmetric JH solutions and merging of symmetric ones were found before a detailed analysis of their stability was made. We think that this precedence was due to the relative simplicity of the bifurcation study of the JH problem, which may be solved using simple analytical methods. Furthermore, the bifurcation analysis is even simpler in the case of free space than in the case of a diverging channel. In contrast to the bifurcation study, the stability analysis, even a linear one, is rather complex in such non-parallel flows and requires careful formulation and interpretation. We prefer to start with simple topics and proceed to more complex and sophisticated cases. This is why we begin with the bifurcation analysis.

3. Bifurcations of primary flows

3.1. *Counting and patterns of the JH solutions*

Many features of the solutions of the JH flow are known through the earlier works mentioned in the Introduction. Here we review some of them for clarity in
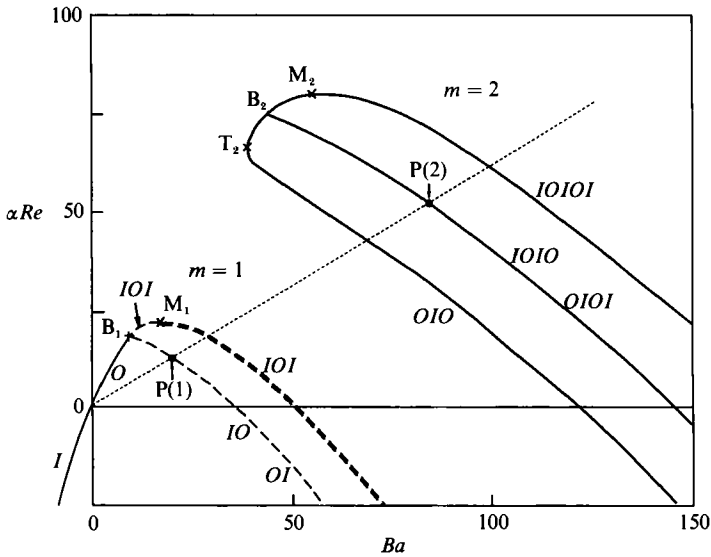
FIGURE 1. Bifurcation diagram for a divergent channel flow with $\alpha = 10°$. Re, Ba relate to the mean and maximum velocities; m denotes the maximum number of outflow regions for each group of solutions. Solutions IO and OI are single-dashed lines because both have one positive eigenvalue, and part of curve IOI is double dashed because corresponding solutions have two positive eigenvalues. As Re increases, asymmetric solutions IO and OI merge and disappear at B_1, and symmetric solutions IOI (single-dashed and double-dashed) merge and disappear at M_1.

presentation of our new results. The JH problem has a countable infinite set of solutions. This 'count' depends upon the choice of a velocity scale. Prior papers have used both the flow rate and the maximum velocity (these two correspond to dimensionless numbers denoted by Re and Ba here). We shall try to answer Batchelor's question (1967, p. 301) on how the number of solutions increases with the maximum velocity. Another reason to re-examine the JH flow is to emphasize similarity properties of the asymmetric JH solutions, and the similarity of bifurcation values at small angles and high Reynolds numbers.

We shall discuss the JH solution features using a parameter plane (Re, Ba). The use of both these parameters allows us to compare our calculations with others'. An additional parameter is the angle α between the walls in the JH flow. Of course, only two of the parameters Re, Ba, α are independent; when any two are fixed the third, as well as the problem solution, can be determined. It is known (Batchelor 1967) that at small α, the solutions are determined not by α and Re separately but by the product αRe (or Ba) only. We have re-examined some of the JH solutions numerically. Calculations results for $\alpha = 10°$ are shown in figure 1. (This angle has been chosen here to compare our numerical calculations with the results of Millsaps & Pohlhausen 1953). Here we use the notation O (outflow) and I (inflow), and their combination allows a compact characterization of the flow pattern (figure 2). We find this notation particularly convenient, and it does not contradict the mathematical classifications (based on features of the elliptic functions) used by Rosenhead and Fraenkel. Patterns IO and OI relate to the full period of the elliptic function, in terms of which all solutions of (4) may be expressed (Hamel 1916). I and O have to alternate: for example, OIO means that, beginning from the lower wall as we move counterclockwise, there are regions of outflow, inflow and outflow successively. It is also convenient to introduce an integer parameter m, which equals the number of full
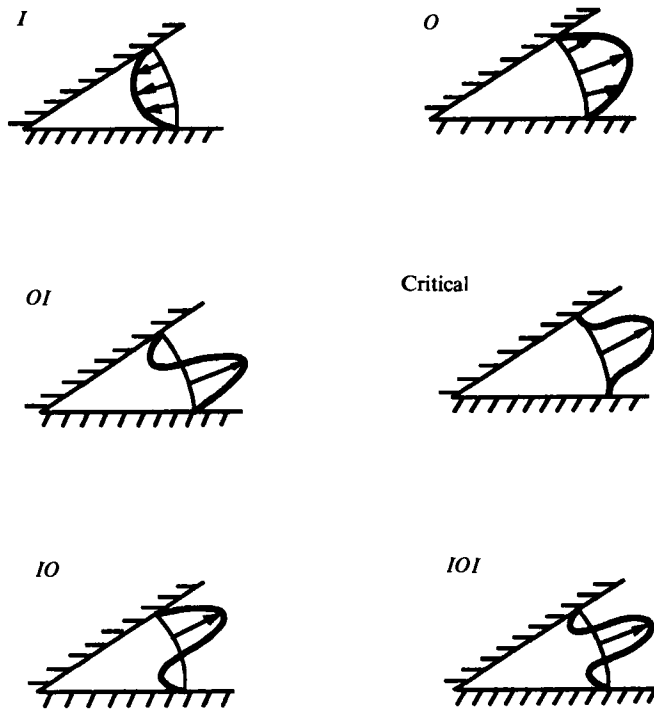
FIGURE 2. Flow pattern of solutions with $m = 1$ in figure 1. The 'critical' distribution which divides the O and IOI solutions is also shown.

periods of the elliptic function in a distribution of $U(\phi)$, $0 \leqslant \phi \leqslant \alpha$, for the asymmetric solutions. Symmetric solutions, connected to these asymmetric solutions by a bifurcation point, are marked by the same value of m.

Branch I in figure 1 corresponds to a pure convergent flow between two inclined planes. As $Re \to -\infty$, the distribution of the radial velocity becomes nearly constant with ϕ, with the boundary layers along the walls becoming thinner. Branch O corresponds to pure divergent flow. As one moves along the branch O from the origin (in the figure), the wall shear stress first increases and then decreases to 0 at B_1. As Re increases, the regime O transforms into the regime IOI at B_1. At the same point a subcritical bifurcation of two asymmetric solutions IO, OI takes place. Both of these regimes correspond to the same dashed curve in figure 1 because they have equal mean and maximum velocities, and one is the reflection of the other with respect to the half-angle plane. In figure 1, B_2 and M_2 can be interpreted the same way as B_1 and M_1; T_2 will be explained in §3.1.2.

These features are in qualitative agreement with the results of Fraenkel (1962), Hooper *et al.* (1982), and Sobey & Drazin (1986). The coordinates of B_1 were found to agree with the asymptotic values, $\alpha Re_* = 18.8$ (Landau & Lifshitz 1986, p. 80) and $Ba_* = 10.31$ (Batchelor 1967, p. 299) for $\alpha^2 \ll 1$ (subscript $*$ in this paper denotes the critical bifurcation value). As $\alpha \to 0$, the divergent channel transforms to a plane channel. Because $Re_* = 18.8/\alpha \to \infty$, such a bifurcation (and instability) is absent in plane Poiseuille flow. But the well-known convective instability occurs in Poiseuille flow, which is more dangerous than the steady instability at very small α (Georgiou & Eagles 1985), because convective instability happens at the finite Reynolds number $Re_* = 7696$ based on the gap size as a lengthscale (see, for instance,

Goldshtik & Shtern 1977). The convective instability becomes more dangerous at $\alpha < 18.8/7696 = 0.7°$. Results of calculations for $\alpha = 10°$ are in good agreement with the asymptotic limit $\alpha \ll 1$ (e.g. $\alpha Re_* = 18.8$). Therefore, there is a rather wide range of the channel angle for which scaling can be used.

3.1.1. *Scaling*

Let us consider an asymmetric solution corresponding to one period of the elliptic function (see *OI* or *IO*, figure 2) for the parameter values, say, α_1 and Re_1. By joining m such channels and removing intermediate walls we obtain a flow for $\alpha_m = m\alpha_1$ and $Re_m = mRe_1$, corresponding to m periods of the elliptic function. It follows that $\alpha_m Re_m = m^2 \alpha_1 Re_1$. Now we use the result that solutions depend on the product αRe only at small α.

In this asymptotic limit there are scaling relations among solutions $(IO)_m$, where $m = 1, 2, \ldots$ and the index means that *IO* is repeated m times. One may produce curve $(IO)_m$ from curve *IO* with the help of the mapping, $P(m) = m^2 P(1)$, where $P(1)$ is a point on the curve *IO* (figure 1) and $P(m)$ is the mapped point on the curve $(IO)_m$. In particular, the same relation is valid for points $B_1, B_2, \ldots,$ and for the parameters corresponding to the bifurcations of the asymmetric regimes; that is

$$Re_*(m) = m^2 Re_*(1); \quad Ba_*(m) = m^2 Ba(1); \quad m = 1, 2, \ldots.$$

Note that in figure 1, such mapping corresponds to rays passing through the origin so that P(1) and P(2) on any rays are related as P(2) = 4P(1). In particular, the distance of B_2 from the origin is 4 times that of B_1. Such a scaling is absent for symmetric solutions because they do not consist of an integer number of periods of the elliptic function. Note that even orientations of curves *OIO* and *O* in figure 1 are different.

3.1.2 *Counting*

An infinite set of solutions exists at each *Re*, but as *Re* increases the asymmetric solution pairs disappear at points B_m due to the subcritical pitchfork bifurcations. The symmetric solution pairs $I(OI)_m$ merge and disappear at points M_m due to the subcritical tangent bifurcations. See also Frankel (1962) and Hooper *et al.* (1982).

The solution set is divided into separated groups, corresponding to different m (see figure 1). Each group consists of four solution branches, which have different flow patterns, but converge at points B_m. Any solution of such a group includes m regions of outflow (except the solution *I* for $m = 1$). For example, the group for $m = 2$ consists of solutions *OIO, IOIO, OIOI, IOIOI*, and any solution has two *O* only.

But if, instead of *Re*, one uses *Ba* as the independent parameter, as Hamel and Batchelor did, then bifurcation features are different. Pitchfork bifurcations at B_m become supercritical; M_m are not bifurcation points now, but T_m (for $m = 2, 3, \ldots,$) are the points where supercritical tangent bifurcations take place. Point T_2 is shown in figure 1.

Batchelor (1967, p. 301) has noted, 'the number of possible distributions increase with αR, although not in a way which can be specified simply'. Batchelor's αR corresponds to *Ba* in our paper and we provide our answer to his remark. *The number of the solutions N equals the number of intersection points of a vertical line Ba = const with the curves in figure* 1. At $Ba < Ba_*(1)$ there is the unique solution, first *I* (at $Ba < 0$) and then *O*. Upon passing B_1, solution *O* transforms into *IOI* and two new solutions *IO* and *OI* appear. The number of solutions, then, increases to 3. At point T_2, owing to supercritical tangent bifurcation, two solutions having pattern *OIO* are
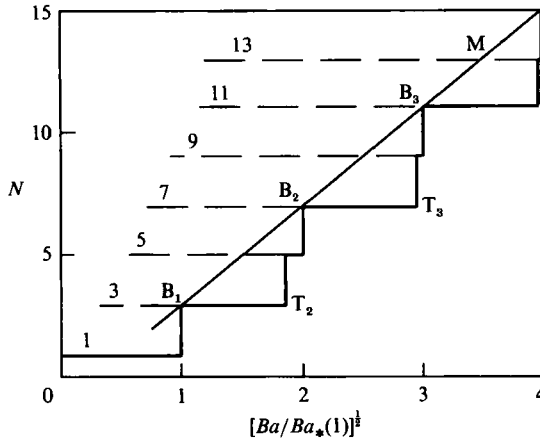
FIGURE 3. Dependence of the JH solution number N on Ba. B_m and T_m are points of pitchfork and tangent bifurcations respectively. The number of solutions after the corresponding bifurcations are indicated in the figure.

added, and N now becomes 5, and so on. At each B_m and at each T_m, two additional solutions appear, so that $N(Ba)$ is the step function shown in figure 3. For all $N \geqslant 1$ this step function is bounded by straight line M, which is described by the relation

$$N = 4[Ba/Ba_*(1)]^{\frac{1}{2}} - 1.$$

As a result of the scaling, i.e. the relation $Ba_*(m) = m^2 Ba_*(1)$, it follows that as Ba increases past $Ba_*(m)$, N becomes $(4m-1)$ for $m = 1, 2, \dots$. This count N remains valid asymptotically for $Ba \gg 1$ even when α is not very small because the value of angle α is bounded: $\alpha \leqslant 2\pi$. However, Ba may become arbitrarily large, so that asymptotically $Ba \gg \alpha^2$ and the relations for points $Ba_*(m)$ remain valid. As α increases, the curves in figure 1 preserve their arrangement qualitatively but move to the left and down (compare figures 1, 21 and 23). At $\alpha = \pi$, point B_1 coincides with the origin (figure 21), and at $\alpha = 2\pi$ point B_2 reaches the origin (figure 23) (Fraenkel 1962). Both of the cases will be considered in the following to model some jet-like flows. At $\alpha = 2\pi$, solutions corresponding to points $Ba_*(m)$ may be considered as free-space flows, because in these critical situations both velocity and shear stress have zero values at the walls (similar to the 'critical' case in figure 2). This is why the walls may be removed. But for the free-space problem, these points are not bifurcation points.

Thus the bifurcation analysis together with the scaling feature allows us to count the number of solutions.

3.2. *Bifurcations in the vortex-source flow*

3.2.1. *Equations for disturbances*

In the free-space problem one may find bifurcations of new solutions analytically. Bifurcation of steady solutions from a pure radial flow in free space has been considered by Goldshtik & Shtern (1989) together with some approximate analysis of unsteady solutions in the vortex-source problem. Here we shall show that steady solutions appear owing to bifurcation in the general case of the potential vortex-source flow. The stream function for this solution is $\Psi_0 = U_0 \phi - V_0 \xi$ with the vorticity $\Omega = 0$ outside the origin. We seek bifurcation of a new steady solution, so

that $\partial/\partial T = 0$ and $\Omega = \Omega_1 (\phi, \xi)$, $\Psi = \Psi_0 + \psi_1 (\phi, \xi)$. Then we obtain from (2) the following system:

$$\frac{\partial^2 \Omega_1}{\partial \phi^2} + \frac{\partial^2 \Omega_1}{\partial \xi^2} - 4\frac{\partial \Omega_1}{\partial \xi} + 4\Omega_1 = U_0\left(\frac{\partial \Omega_1}{\partial \xi} - 2\Omega_1\right) + V_0\frac{\partial \Omega_1}{\partial \phi} + \frac{\partial \psi_1}{\partial \phi}\left(\frac{\partial \Omega_1}{\partial \xi} - 2\Omega_1\right) - \frac{\partial \psi_1}{\partial \xi}\frac{\partial \Omega_1}{\partial \phi};$$

$$(7a)$$

$$\frac{\partial^2 \psi_1}{\partial \phi^2} + \frac{\partial^2 \psi_1}{\partial \xi^2} = \Omega_1. \tag{7b}$$

3.2.2. *Linear analysis*

The necessary condition for bifurcation is the existence of a non-trivial solution of the linearized equation. Therefore, we first linearize this system, neglecting the nonlinear terms in (7a). Because all coefficients of the linearized system are constant, solutions may be sought in the normal form: $\Omega_1 = \exp[im(\phi - \beta\xi)]$. Then from (7a), which becomes decoupled from (7b), we obtain the dispersion relation

$$(1 + \beta^2) m^2 + im[V_0 - \beta(U_0 + 4)] - 2U_0 - 4 = 0. \tag{8}$$

It follows that $$\beta = V_0/(U_0 + 4); \tag{9}$$

$$m^2 V_o^2 = (U_0 + 4)^2 [2U_0 + 4 - m^2]. \tag{10}$$

Expression (10) gives the relation between the radial and azimuthal velocities U_0 and V_0, and this is the necessary condition for bifurcation. These 'neutral' curves are shown in figure 4, where $V_0 = 0$ is a symmetry axis. The bifurcational values of U_0, V_0, satisfying (10) will be denoted by U_{0*}, V_{0*}.

3.2.3 *Nonlinear analysis*

The neutral modes of the linear theory depend on ϕ and ξ, but through a single argument $\chi = \phi - \beta\xi$. Using an expansion method with a small parameter of amplitude $\epsilon = A$ or the U_0 displacement $\epsilon^2 = U_{0*} - U_0$, one can easily find that nonlinear neutral disturbances also depend only on χ. Therefore we seek solutions in the following form:

$$\Psi = U_0\phi - V_0\xi + (1 + \beta^2) \psi(\phi - \beta\xi). \tag{11}$$

The existence of such a class of Navier–Stokes equation solutions had been pointed out by Oseen (1927). Our new observation is that solutions of this class bifurcate from the potential vortex source; we also discuss features of some such solutions and their interpretation. Substitution of (11) into (2) yields the following ordinary differential equation for $\psi(\chi)$:

$$\psi^{\mathrm{iv}} + \hat{\nu}\psi''' + \mu\psi'' = -2\psi'\psi'';$$

where $$\hat{\nu} = \frac{\beta(4 + U_0) - V_0}{1 + \beta^2}, \quad \mu = \frac{4 + 2U_0}{1 + \beta^2};$$

and the prime denotes differentiation with respect to χ.

Using $\psi' = u$ and integrating, one gets

$$u'' + \hat{\nu}u' + \mu u = C - u^2. \tag{12}$$

For physical reasons, solution $u(\chi)$ must be a periodic function of χ with period 2π. Multiplying (12) by u' and integrating in the interval $0 \leqslant \chi \leqslant 2\pi$ we obtain

$$\hat{\nu}\int_0^{2\pi} (u')^2 \mathrm{d}\chi = 0.$$

We look for a non-trivial solution, which requires that $\hat{v} = 0$. Then, $\beta = V_0/(U_0+4)$; this coincides with (9), but is valid in a general nonlinear case. Thus in (11) the parameter β is a function of U_0 and V_0. In the nonlinear case also, U_0 and V_0 are radial and azimuthal velocities averaged over angle ϕ. Then the averaged value of u has to be zero, i.e.

$$\int_0^{2\pi} u \, \mathrm{d}\chi = 0; \quad C = \int_0^{2\pi} u^2 \, \mathrm{d}\chi \geqslant 0.$$

The latter relation follows from the integration of the equation

$$u'' + \mu u = C - u^2. \tag{13}$$

If one chooses the position of a local maximum of a periodic function $u(\chi)$ as the origin in the χ-axis, then solutions of (13) would satisfy the initial conditions

$$u(0) = A; \quad u'(0) = 0. \tag{14}$$

Here A, being the maximum value of $u(\chi)$, is considered to be a new parameter. All solutions of this initial-value problem for any tentative A, μ and C are symmetric with respect to the positions of their extrema. That is why it is sufficient to satisfy $u'(2\pi) = 0$ with $u''(2\pi) < 0$; the second condition of periodicity, $u(2\pi) = A$, would be satisfied automatically. Thus we have the two conditions:

$$u'(2\pi) = 0, \quad \int_0^{2\pi} u \, \mathrm{d}\chi = 0; \tag{15}$$

which must be satisfied by a selection of the parameters A, μ and C. It is convenient to consider the amplitude A as a free parameter and to find μ and C by the method of shooting to satisfy conditions (15). To reiterate, we started with the problem having two free parameters U_0, V_0 and have reduced it to the problem (13)–(15) with only one free parameter A.

For the case $m = 1$, we can find this one-parameter set of solutions $\{u_1(\chi, A_1),$ $\mu_1(A_1), C_1(A_1)\}$ in the whole interval $0 \leqslant A_1 \leqslant \infty$, then solutions for an arbitrary m can be obtained by the scaling transformations:

$$A_m = m^2 A_1; \quad \mu_m = m^2 \mu_1; \quad C_m = m^4 C_1; \quad u_m(\chi) = m^2 u_1(m\chi).$$

3.2.4. *Small-amplitude expansion*

For $A = 0$, the solution of (13)–(15) is trivial (i.e. $u \equiv 0$, $C = 0$). To study what kind of bifurcation takes place, we use the expansions

$$u = Au_1 + A^2 u_2 + A^3 u_3 + \dots; \quad C = A^2 C_2 + A^3 C_3 + \dots; \quad \mu = \mu_0 + A\mu_1 + A^2 \mu_2 + \dots.$$

It follows from (13) that $u_1'' + \mu_0 u_1 = 0$, and (14) and (15) yield

$$\mu_0 = m^2; \quad u_1 = \cos(m\chi).$$

At the second order of A, we have from (13),

$$u_2'' + m^2 u_2 = C_2 - \cos^2(m\chi) - \mu_1 \cos(m\chi).$$

The right-hand side must be orthogonal to $\cos(m\chi)$; consequently, $\mu_1 = 0$. From the second condition (15) we obtain $C_2 = \frac{1}{2}$ and
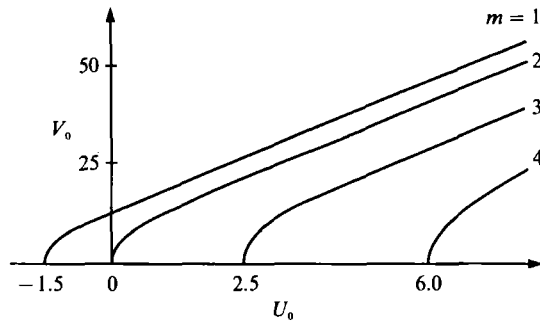
$$u_2'' + m^2 u_2 = -\frac{1}{2}\cos(2m\chi).$$

FIGURE 4. Curves of bifurcations in the vortex-source flow. U_0 and V_0 are proportional to the flow rate and circulation, m is the number of angular oscillations in the velocity distribution.

Because of (14), the solution of the above equation is

$$u_2 = [\cos(2m\chi) - \cos(m\chi)]/(6\,m^2).$$

At the third order, we have

$$u_3'' + m^2 u_3 = -2u_1 u_2 - \mu_2 u_1 + C_3$$

$$= \frac{\cos(2m\chi) - 1 - \cos(m\chi) - \cos(3m\chi)}{6m^2} - \mu_2 \cos(m\chi) + C_3.$$

The orthogonality condition and (15) give

$$\mu_2 = -1/6m^2; \quad C_3 = 1/6m^2.$$

Therefore, μ decreases with increasing A near the bifurcation point. Then we use the relations

$$\beta = \frac{V_0}{U_0 + 4}, \quad \mu = \frac{4 + 2U_0}{1 + \beta^2}; \tag{16}$$

to calculate derivative $\partial\mu/\partial U_0$ at fixed V_0, i.e.

$$\frac{\partial\mu}{\partial U_0} = \frac{2}{1 + \beta^2}\left[1 + \frac{\beta^2(4 + 2U_0)}{(1 + \beta^2)(U_0 + 4)}\right].$$

It follows from (10), as one can also see in figure 4, that $U_{0*} \geqslant -\frac{3}{2}$. Therefore, $(\partial\mu/\partial U_0)_* > 0$, where the asterisk denotes the derivative at the 'neutral' curves. Then at $A = 0$, because of

$$0 > \mu_2 = \frac{\partial\mu}{\partial A^2} = \frac{\partial\mu}{\partial U_0}\frac{\partial U_0}{\partial A^2},$$

we find that U_0 decreases with increasing A; i.e. the bifurcation is subcritical with respect to U_0 at any fixed V_0 and m. In particular, for $V_0 = 0$,

$$U_0 = U_{0*} - \frac{A^2}{12\,m^2} + O(A^4). \tag{17a}$$

This particular case has been studied by Goldshtik & Shtern (1989). It is helpful for the following discussion to reproduce the results of their calculation, shown in figure 5. There $\Delta U = U_{\max} - U_{\min}$ corresponds to the maximum variation of the
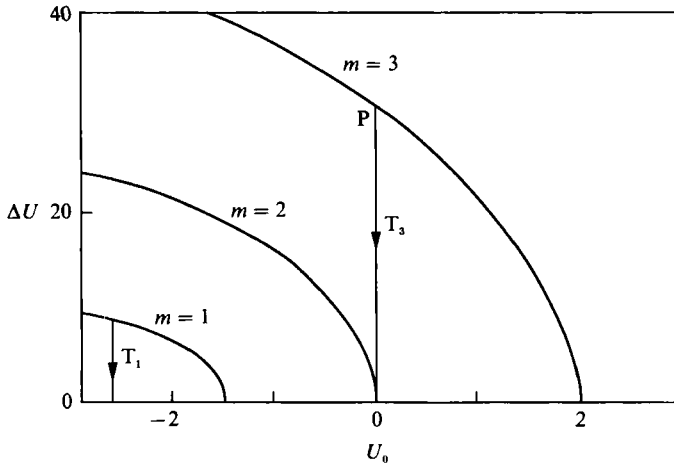
FIGURE 5. Bifurcation diagram for the source flow. ΔU is angular variation of radial velocity. T_1 and T_3 are examples of transition trajectories.

radial velocity as a function of the angle. Near the bifurcation points, which correspond to $U_{0*} = \frac{1}{2}(m^2-4)$ (or $Re_* = \pi(m^2-4)$), we find that $\Delta U = 2A + O(A^2)$, and according to (17a), all the curves in figure 5 are normal to the abscissa at the bifurcation points. To summarize, at any value of the Reynolds number, a countable set of the angular-dependent solutions exists. This feature is common to free-space and divergent-channel problems. The origin in the plane (U_0, V_0) is a bifurcation point and in its vicinity two solutions of arbitrarily small norm coexist: one is uniform and the other is angular dependent.

3.2.5. *Qualitative and asymptotic analyses*

Equation (13), with the help of the transformations

$$u = ay(\theta)+u_1, \quad u_1 = \frac{1}{2}[(\mu^2+4C)^{\frac{1}{2}}-\mu], \left.\begin{array}{c} \\ \\ \end{array}\right\} \tag{17b}$$
$$\theta = \gamma\chi, \quad \gamma = (\mu+2u_1)^{\frac{1}{2}}, \quad a = \frac{1}{2}\gamma^2;$$

may be reduced to the canonical equation for a conservative oscillator with quadratic nonlinearity:

$$y'' + y + \frac{1}{2}y^2 = 0. \tag{18}$$

The first integral of this equation is $y'^2 = E - y^2 - \frac{1}{3}y^3$ where E is an integration constant related to the energy of the oscillator. The phase diagram is shown in figure 6. The trivial solution (for a potential vortex-source) corresponds to the nonlinear oscillator at rest, i.e. $E = 0$, $y = y' = 0$, which is the origin in figure 6. The angle-dependent solutions correspond to the closed orbits filling the region inside the loop of the separatrix which is shown by the thick line (figure 6),

$$y_S = 3\operatorname{sech}^2(\tfrac{1}{2}\theta) - 2; \quad E = \tfrac{4}{3}. \tag{19}$$

One turn along an orbit in figure 6 corresponds to a periodic solution of (13) with azimuthal number $m = 1$. For an arbitrary m, one must go around m times. In terms of the phase diagram each bifurcation means that a small circle appears near the origin. Its scale grows with increasing amplitude and tends asymptotically toward
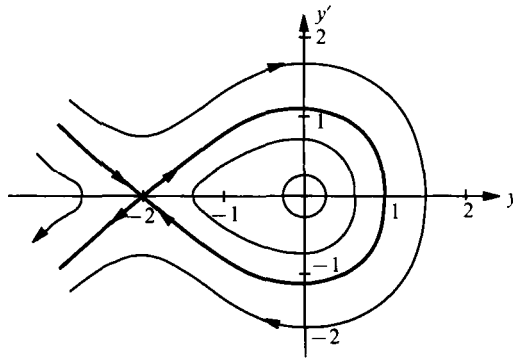
FIGURE 6. Phase plane of the canonical equation (18). Separatrix is shown by a thick line.
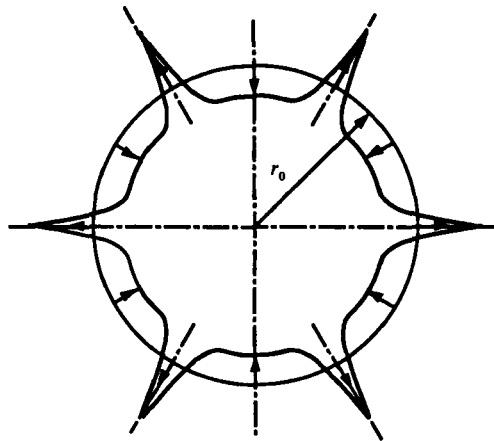

FIGURE 7. Radial outflow and inflow velocity distributions at $r = r_0$ for the secondary flow with $m = 6$.

the separatrix. The distribution $y(\theta)$ changes from harmonic to a nearly constant distribution with a spike in each period and tends to the form (19) as the amplitude $u(0) \to \infty$.

Let V_0 be bounded and $U_0 \to -\infty$. Then from (16) it follows that $\beta \to 0$, and $\mu \to 2U_0 + 4$. Because $u(\chi)$ is nearly constant with zero mean value, $C \to 0$. Further, at the largest order, $u_1 = -2U_0$; $a = -U_0$; $\gamma = (-2U_0)^{\frac{1}{2}}$. It follows from (11) that the radial velocity $U = \partial\psi/\partial\phi = U_0 + u = U_0 + ay + u_1$. As $U_0 \to -\infty$, $y \to y_S$ and from (19), max $(y_S) = 1$; and min $(y_S) = -2$. Therefore, asymptotically, min $(U) = U_0$; and max $(U) = -2U_0$. In other words, the maximum outflow velocity equals twice the maximum inflow velocity.

Let us estimate the width of the outflow region. At its boundary, $U = 0$, this asymptotically corresponds to $y_S = -1$. Then the width is $4z_*|U_0|^{-\frac{1}{2}}$, where $z_* = $ arccosh $\sqrt{3}$. An example of the radial velocity distribution with $m = 6$ is shown in figure 7. The JH solutions can also be interpreted with the help of the phase diagram in figure 6. Equation (4) is reduced to (18) by the transformations in (17b) using a value of $\mu = 4$, where u is replaced by U (compare (4) and (13)). The zero value of U corresponds to $y_0 = -1 + 2(C+4)^{-\frac{1}{2}}$. Intersections of the vertical line $y = y_0$ with an orbit (which depends on the value of C) in figure 6 gives points corresponding to walls of the channel. The everywhere-divergent solution O relates to a part of a closed orbit
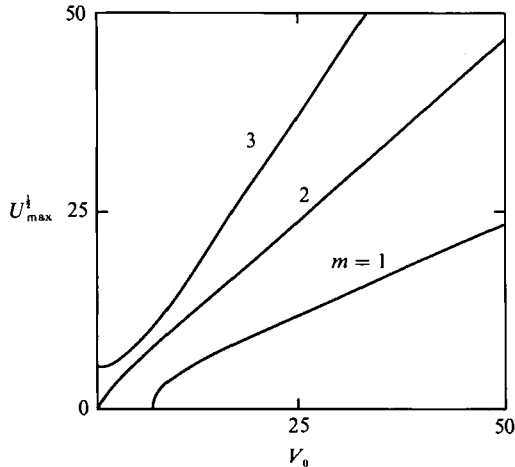
FIGURE 8. Bifurcation diagram for the asymmetric vortices. U_{max} is the maximum value of radial velocity at fixed r.

on the right of $y = y_0$, and everywhere-divergent orbit I relates to the left part of the same orbit. Solution IO relates to the full orbit that starts in the lower intersection point, and OI is the same but starts in the upper point. Other solutions relate to the same orbit with more than one turn. Bifurcation points B_m (figure 1) correspond to the situation when the left side of the orbit touches the line $y = y_0$.

Thus, we see that due to the bifurcations, a countable infinite set of the secondary solutions are generated and flow patterns develop with thin outflow branches separated by wider inflow regions.

3.3. *Asymmetric vortices*

Now we consider the special class of the secondary steady solutions when the flow rate is zero (i.e. $U_0 = 0$). Such solutions are generalizations of the potential vortex flow and include not only the vortex singularity in the origin but also a vortex 'atmosphere' (i.e. distributed vorticity) in which vorticity depends on the radius and the angle. We hope that these solutions, besides being of intrinsic interest, would serve as the simplest models of elementary events of vorticity dynamics in real flows.

In the case $U_0 = 0$ the dispersion relations (9) and (10) are reduced to

$$\beta = \tfrac{1}{4}V_0; \quad m^2 V_0^2 = 16 \ (4-m^2).$$

From the second formula above, it follows that only two bifurcations are permitted for the potential vortex relating to azimuthal numbers $m = 1$ and $m = 2$. Since all results are symmetric with respect to the sign of V_0, it is sufficient to consider $V_0 \geqslant 0$ only. To study the nature of bifurcation (subcritical or supercritical) that takes place, one may use the results of the preceding section with the relation $V_0^2 = 64/\mu - 16$ which follows from (16) for $U_0 = 0$. Then, for $m = 1$, we obtain, (noting that $\mu = \mu_0 + A\mu_1 + A^2\mu_2 + \ldots = m^2 - A^2/(6m^2) + O(A^4)$)

$$V_0 = V_{0*}(1 + \tfrac{1}{9}A^2) + O(A^4), \quad V_{0*} = \sqrt{48};$$

and for $m = 2$, $\qquad V_{0*} = 0; \quad V_0 = A/\sqrt{6} + O(A^3).$

These bifurcations are shown in figure 8 where $U_{max} = (1 + \beta^2)A$ (from (11) using $u_{max} = A$) corresponds to the maximum of the radial velocity at a fixed distance r. As V_0 increases, supercritical bifurcations occur for modes $m = 1, 2$. Bifurcation for
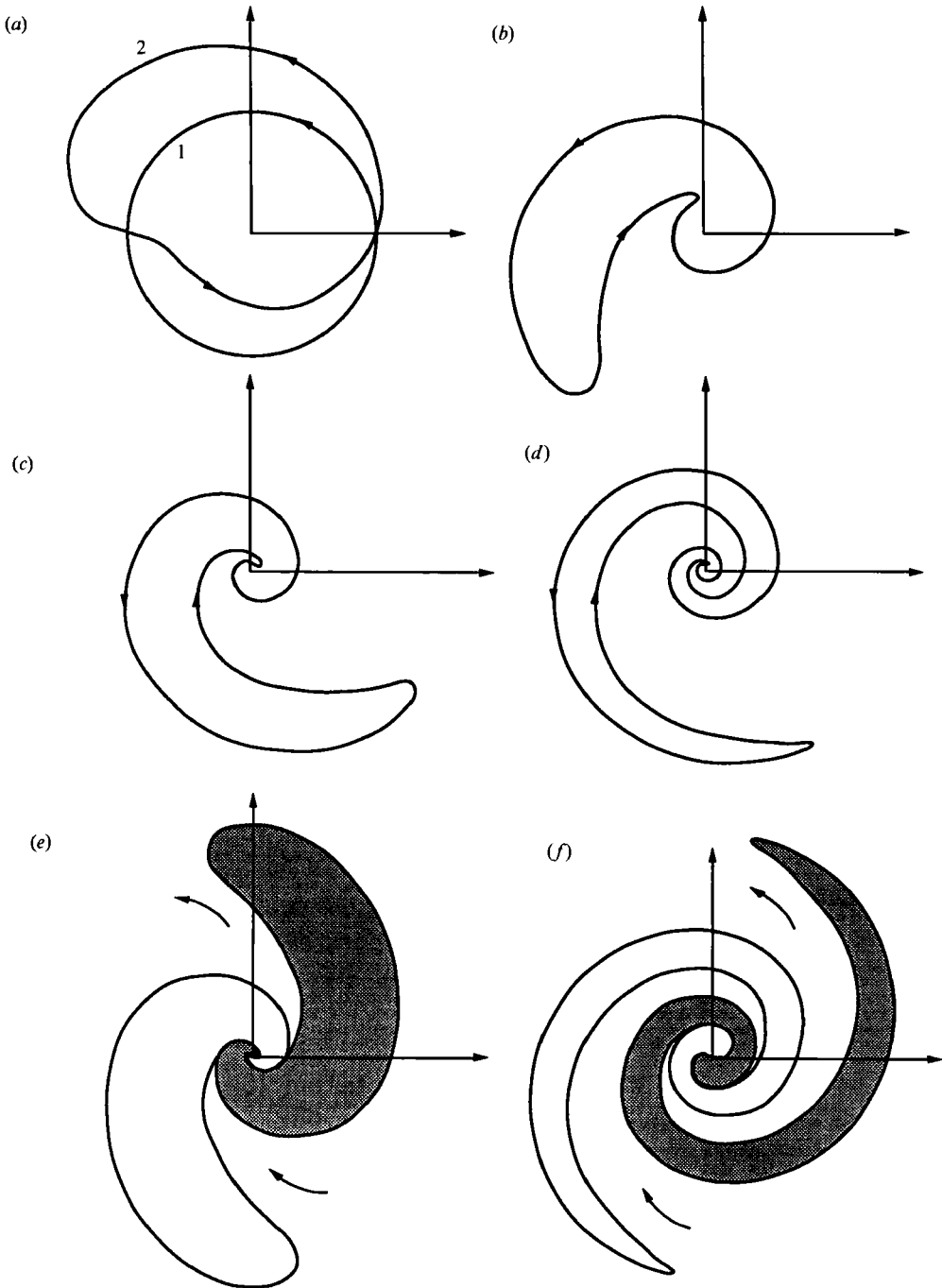
FIGURE 9 (*a–f*). For caption see facing page.

$m = 2$ is degenerate owing to the symmetry of the transformation $V_0 \rightarrow - V_0$. Besides, there is a countable set of curves $m = 3, 4, \ldots$ (only the curve for $m = 3$ is shown in figure 8) corresponding to the solutions which are separated from the potential vortex (corresponding to the abscissa in figure 8) but they all bifurcate from some potential vortex-source flow at some non-zero value of U_0.
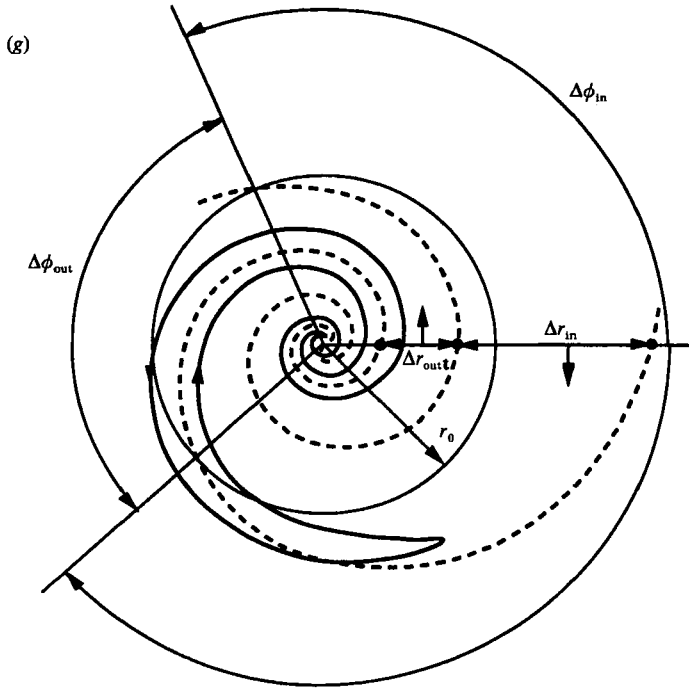
FIGURE 9. Spiral pattern development with the circulation increase for $m = 1$. Streamlines: (a) curve 1, $A = 0$ (base flow); curve 2, $A = 1$, $V_0 = 7.56$; (b) $A = 2$, $V_0 = 9.5$; (c) $A = 2.5$, $V_0 = 11.5$; (d) $A = 3$, $V_0 = 15.4$. Isovorticity lines: (e) and (f) correspond to the same parameters as curve 2 in (a) and case (d) respectively. (g) An enlarged version of (d) including explanations of Δr_{out}, Δr_{in}; $\Delta \phi_{\text{out}}$ and $\Delta \phi_{\text{in}}$ corresponding to $r = r_0$; the dashed lines are lines of zero radial velocity.

Flow patterns for the asymmetric viscous vortices with $m = 1$ are shown in figure 9. To understand the flow patterns, it is sufficient to observe one streamline, say, $\Psi = 0$, because other streamlines are similar. Indeed, from (11) it follows that if $r = r_0 (\phi)$ is the streamline $\Psi = 0$, then other streamlines are related to it by the transformations $r \Rightarrow r_0 \exp(-\Psi/V_0)$, $\phi \Rightarrow \phi - \frac{1}{4}\Psi/4$; these represent uniform scaling and turning (figure 10c).

Curve 1 in figure 9(a), which is a circle, is a streamline of the undisturbed potential vortex, but curve 2 corresponds to the secondary solution. As the amplitude A (and hence V_0) increases, the streamline becomes curved, folded, longer and thinner: compare figure 9(a with b–d). Note that figure 9(e) and curve 2 in figure 9(a) are for the same flow, as is also the case in figure 9(d and f); the creation of the negative-signed vorticity is interesting but obvious. Isovorticity contours are shown in figures 9(e, f). It follows from (11) that $\Omega = (1 + \beta^2)^2 \psi''(\chi)$.

According to the definition $\omega = \Omega \nu / r^2$, we have

$$\frac{r^2}{r_0^2} = \frac{\nu}{\omega r_0^2} \psi'' \left(\phi - \beta \ln \frac{r}{r_0} \right).$$

For $|A| \ll 1$ the isovorticity lines are described by the relation $(r/r_0)^2 \sim A \sin(\chi)$. The region inside a contour of positive vorticity is shaded. Flow direction between the region is shown by arrows. Regions of positive and negative vorticity are separated by the logarithmic spiral lines $\chi = \chi_*$, where χ_* values are such that
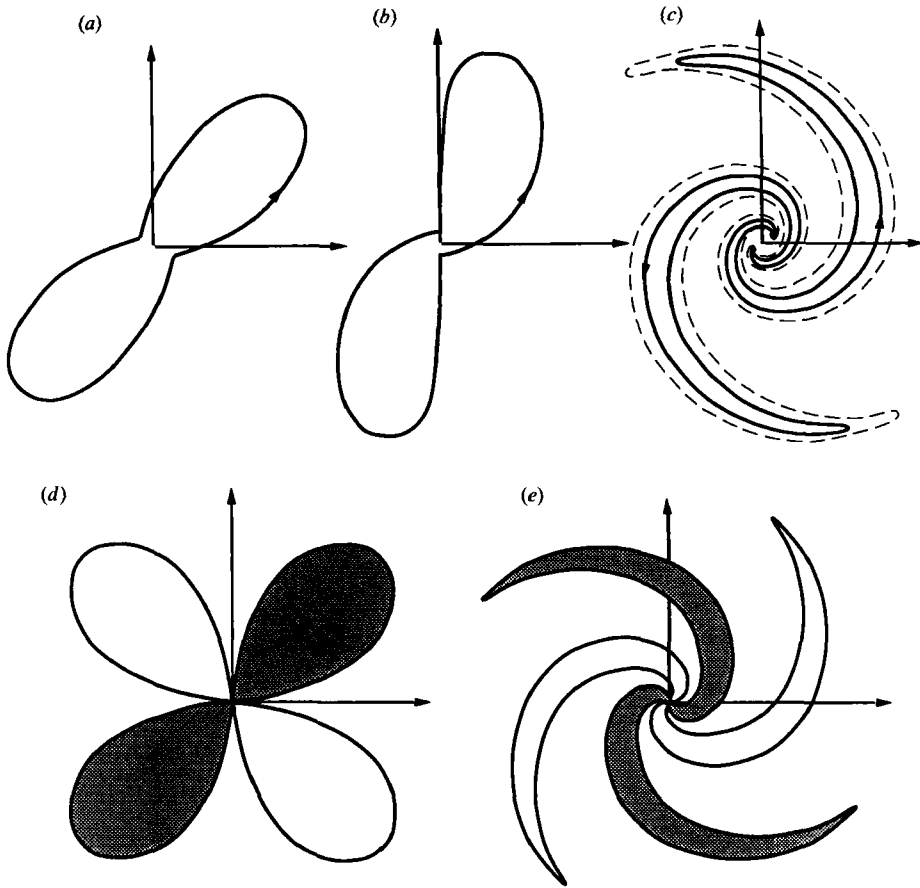
FIGURE 10. Streamlines and isovorticity lines for $m = 2$. Streamlines: (a) $A = 0.1$, $V_0 = 0.041$; (b) $A = 5, V_0 = 1.89$; (c) $A = 13.5$, $V_0 = 11.5$ (dashed curves in (c) denote streamlines for one non-zero value of the stream function). Isovorticity lines: (d) $A = 0.5$, $V_0 = 0.2$; (e) $A = 12$, $V_0 = 6.88$.

$\psi''(\chi_*) = 0$. Note that the vorticity field has a delta-function distribution at the origin. Such a singularity can be thought of as being supported by the rotation of a needle at the origin. If the needle is removed, then the flow becomes unsteady (diffusive), depending on $\nu t/r^2$. The first effect of diffusion would be a smoothing of the delta-distribution to the Gaussian distribution. This leads to the appearance of a core of positive vorticity peaked at the origin and extending outward by a rather thin spiral branch.

Some results for $m = 2$ are shown in figure 10. In the limit $A = 0$, (using (11)) the streamline $\psi = 0$ is given by the relation,

$$r = r_0 \exp\left[\left(\tfrac{3}{2}\right)^{\frac{1}{2}} \sin\left(2\phi\right)\right].$$

This pattern is close to the curve in figure 10(a). As A increases, the streamline becomes more like a spiral, as seen in figure 10(b, c). The isovorticity contours are shown in figures 10 (d, e). Replacing the delta-function with the Gaussian distribution, we obtain a quasi-steady picture of the merging of two vortical patches – a typical event in shear layers and jet-like flows.

Streamlines for the solution family with $m = 3$ are shown in figure 11. This family
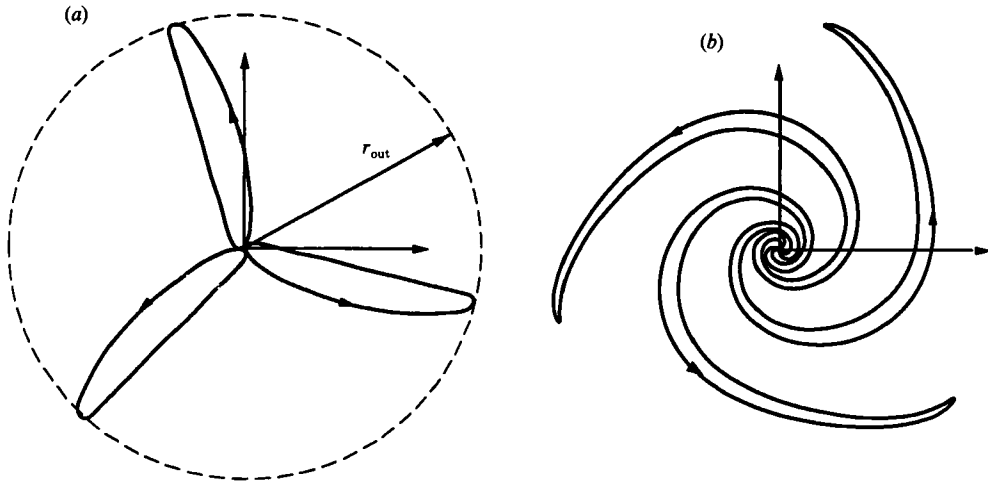
FIGURE 11. Streamlines of the asymmetric vortices with $m = 3$: (a) $A = 22.5$, $V_0 = 0.62$; (b) $A = 31.5$, $V_0 = 10.2$.

does not bifurcate from the potential vortex (figure 8). At $V_0 = 0$ there is a pure radial flow with zero total flow rate. This case corresponds to the intersection point of the curve for $m = 3$ and line T_3 in figure 5. This flow consists of three sectors of outflow ('jets') and three sectors of inflow. For $V_0 \neq 0$ all streamlines become closed and each of them is placed inside a ring $r_{min} < r < r_{max}$. In particular, for the streamline $\Psi = 0$,

$$r_{max}/r_{min} = \exp\left[(1+\beta^2)(\psi_{max} - \psi_{min})/V_0\right].$$

For $V_0 \to 0$, the value of $(\psi_{max} - \psi_{min})$ has a finite non-zero limit corresponding to pure radial flow, and r_{max}/r_{min} tends to infinity. Therefore, streamlines in figure 11 do not touch the origin but come very close to it. Isovorticity lines are not shown because they are similar to those in figure 10, but consist of three branches. The existence of regions of negative vorticity is explained by the jet-like character of the flow; this feature is the main difference between the viscous flows we discuss here and the vortex patch structures in ideal fluid reviewed by Aref (1983).

Because $\mu = 64/(V_0^2 + 16)$ we have $\mu \to 0$ when $V_0 \to \infty$. At $\mu = 0$ and $m = 1$, the problem (13)–(15) has the solution $A_\infty = 3.649$ and $C_\infty = 3.333$. The corresponding distribution $u(\chi)$ is shown in figure 12, with $u_{max} = A_\infty$, $u_{min} = -1.716$ and $\chi_0 = 1.2$ such that $u(\chi_0) = 0$. At a fixed r, the width $\Delta\phi_{out}$ of the outflow region and the width $\Delta\phi_{in}$ of the inflow region are related by the so-called Golden Mean:

$$\Delta\phi_{out}/\Delta\phi_{in} = \tfrac{1}{2}(\sqrt{5} - 1) \approx 0.62.$$

The width of the outflow region measured in the radial direction is $\Delta r_{out} = 2\chi_0 r/\beta$. Because

$$V = V_0 + (1+\beta^2)\beta u, \quad \beta = \tfrac{1}{4}V_0, \quad U = (1+\beta^2)\,u,$$

the amplitude of the oscillating part of V is significantly larger than the uniform part of V for $V_0 \gg 1$, the radial velocity is small compared to the azimuthal velocity and the streamlines diverge very weakly. Let $v_{\phi 0}$ be a dimensional value of the uniform part V_0 of the azimuthal velocity. Using $V_0 = v_{\phi 0} r/\nu$ we have,

$$\Delta r_{out} = 8\chi_0 \nu/v_{\phi 0}.$$
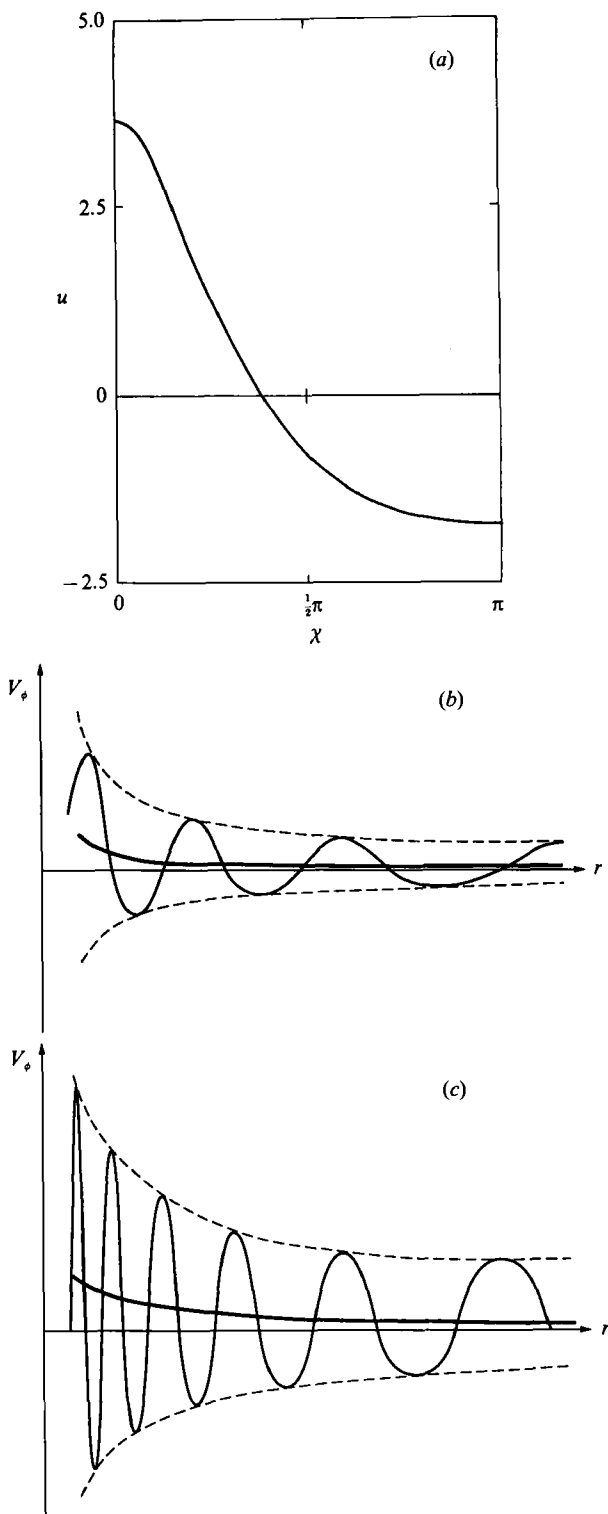
FIGURE 12. (a) Asymptotic (as $V_0 \to \infty$) form of velocity distribution in the asymmetric vortices. (b, c) Radial variation of the azimuthal velocity; V_0 is higher in (c) than in (b). Note amplitude and frequency variation with V_0, as well as with r. Non-oscillating part $(\nu V_0/r)$ and oscillating part are denoted by thick and thin lines respectively.

If $v_{\phi 0}$ is fixed and $\nu \to 0$, then $\Delta r_{\text{out}} \to 0$. But at fixed ν, Δr_{out} increases in proportion to the distance r. The oscillating dimensional velocity tends to infinity as $\nu \to 0$:

$$\frac{v_\phi}{v_{\phi 0}} = \frac{r^2 v_{\phi 0}^2}{64 \nu^2} u(\chi); \quad \frac{v_r}{v_{\phi 0}} = \frac{r v_{\phi 0}}{16 \nu} u(\chi).$$

Thus, in the limit of $\nu \to 0$, we obtain a superposition of a potential vortex of bounded circulation and a velocity field oscillating in space with infinitely large amplitude and having infinitely small wavelength in the radial direction (schematically shown in figure 12b, c).

To summarize, in this section non-axisymmetric steady solutions of the Navier–Stokes equation were found which bifurcate from the potential vortex-source flow. To obtain these solutions, we used the methods of bifurcation theory, but did not need to employ any stability analysis. We suggest that such solutions may be useful irrespective of whether they are stable or unstable. There are many examples of dynamical systems spending a rather long time near saddle points. One such gives the phase diagram shown in figure 6 where a marked point would 'move' slowly near the saddle point $y = -2$, $y' = 0$ and faster far away from this point. If transitions between saddles are quick and passages near these trajectories are long, then the saddle trajectories may be viewed as 'coherent structures' in a chaotic motion.

However, it is very important to know the stability features of the solutions and values of the growth rate. Bifurcation is intimately related to stability, and as a rule, bifurcation occurs with a change in the stability features of an initial solution. This brings us to the stability study discussed in the next section.

4. Stability of the solutions

4.1. *The approach*

The stability features of the solutions which we have obtained and considered above and, in particular, of the potential vortex source, are rather surprising. Therefore, the problem deserves a careful analysis as well as simple and clear formulation. We look for a perturbed solution of the form

$$\Psi = \Psi^0 = \psi_1(\phi, \xi); \quad \Omega = \Omega^0 + \Omega_1(\phi, \xi); \tag{20}$$

where Ψ^0, Ω^0 correspond to a base solution whose stability we wish to study. In the case of the vortex source, $\Psi \equiv \Psi_0$, $\Omega^0 \equiv \Omega_0 = 0$.

In general, the disturbances ψ_1 and Ω_1 may also depend on T. One can see that if equations (1) are linearized with respect to the disturbances, they permit solutions proportional to $\exp(\lambda t)$; but coefficients of the linearized equations depend on r and ϕ, so that it is necessary to solve a two-dimensional problem (for eigenvalues and eigenfunctions).

In special cases, the problem may be simplified using the multi-scale approach and expansion with respect to a small parameter. Such a parameter may be a scale ratio of disturbance wavelength and a distance at which the base flow changes significantly. This has been done for the JH flow by Giorgiou & Eagles (1985, see also references therein). But in the case where the angle between the walls is not small or in the free-space problem, we do not know in advance if scales of a base flow differ enough from scales of amplifying disturbances to justify the use of the multi-scale approach. This is one reason why we prefer to avoid such an expansion approach here.

In Goldshtik & Shtern (1989), self-similar time-dependent disturbances were studied which permit, in the two limiting cases $T \to -\infty$ and $T \to \infty$, a decomposition

in terms of the normal modes. We are not satisfied with these results because the assumptions used are questionable and their interpretations present some difficulties. In this paper we prefer to use mainly a spatial stability approach. For the JH flow such an approach has been widely followed beginning with Dean (1934) and continuing to the present (Banks *et al.* 1988). Here we study the spatial stability of the vortex-source flow and the secondary solutions, as well as new stability features of the JH flow, regarding the appearance of complex-conjugate pairs of eigenvalues.

Substituting (20) in (2) we obtain, for $\partial/\partial T = 0$, the equations for disturbances

$$
\left.
\begin{aligned}
&\frac{\partial^2 \psi_1}{\partial \phi^2} + \frac{\partial^2 \psi_1}{\partial \xi^2} = \Omega_1, \\
&\frac{\partial^2 \Omega_1}{\partial \phi^2} + \frac{\partial^2 \Omega_1}{\partial \xi^2} - 4\frac{\partial \Omega_1}{\partial \xi} + 4\Omega_1 = U^0 \left(\frac{\partial \Omega_1}{\partial \xi} - 2\Omega_1\right) + V^0 \frac{\partial \Omega_1}{\partial \phi} \\
&\qquad\qquad\qquad\qquad + \frac{\partial \psi_1}{\partial \phi}\left(\frac{\partial \Omega_1}{\partial \xi} - 2\Omega_1\right) - \frac{\partial \psi_1}{\partial \xi}\frac{\partial \Omega_1}{\partial \phi};
\end{aligned}
\right\}
\tag{21}
$$

which differ from (7) only by the substitutions $U^0 \to U_0$ and $V^0 \to V_0$. In this section we study infinitesimal disturbances so that the nonlinear terms in (21) are neglected. We consider the cases when coefficients of the linearized equations (21) depend only on ϕ and not on ξ. Therefore, we seek solutions in the normal form

$$
\psi_1 = \Phi(\phi) \exp(\lambda \xi); \quad \Omega_1 = \zeta(\phi) \exp(\lambda \xi).
$$

The problem is then reduced to

$$
\zeta'' + V\zeta' + (k^2 - kU)\zeta + 2U'\Phi' + \lambda U''\Phi = 0; \quad \Phi'' + \lambda^2 \Phi = \zeta, \quad k = \lambda - 2, \tag{22\,a, b}
$$

where the superscript '0' for U and V is omitted.

The eigenvalues λ can be found from the requirement that a non-trivial solution of (22) exists and satisfies the periodicity conditions (for the free-space case) or the non-slip conditions (for the channel case).

Now we shall discuss the behaviour of small disturbances near the origin and at infinity. Because $\exp(\lambda \xi) = (r/r_0)^\lambda$, one can see that if λ_r, the real part of λ, is negative, then such a disturbance has a stronger singularity at the origin than the base solution. Therefore, there is a question as to whether the linear analysis is applicable in the near-origin region. To avoid this difficulty we assume that the disturbed velocity field, say the ψ_1 and Ω_1 distributions, is given at some fixed distance $r = r_0$, and see how the disturbances develop with increasing r. In the case $\lambda_r < 0$ the disturbance decays faster than the base flow. We may interpret this as the spatial stability of the base flow with respect to such a disturbance.

If $\lambda_r > 0$, the base flow is expected to be unstable, but there is another difficulty. It is known that for the JH problem, even at $Re = 0$ a countable set of eigenvalues λ exists with $\lambda_r > 0$ (see Banks *et al.* 1988 and references therein). It will be shown that the same is true for the free-space problem. In particular, there are modes for which λ_r increases and tends to infinity when the scale of the disturbance decreases to zero. On the physical grounds that small scales have large dissipation and must decay, such eigenvalues and modes must be considered irrelevant. These difficulties are brought about by our attempt to solve the initial-value problem for disturbances instead of solving a boundary-value problem for the elliptic equations with boundary conditions at infinity (Banks *et al.*). The selection of relevant modes is a rather sophisticated problem in general (for spatial disturbances of the plane Poiseuille flow see discussions by Goldshtik & Shtern 1977, p. 133). We shall use a method of

selection that involves a continuation of parameter values. First, we consider a rather simple flow, which is clearly stable for physical reasons, and identify the relevant and irrelevant modes. We then study dependence of eigenvalues for the relevant modes on parameter values. That is, instability occurs if λ_r becomes positive for one of the relevant modes. Such an approach is the simplest, as is obvious in the case of the potential vortex-source flow.

4.2. Stability of the vortex-source flow

In this case $U \equiv U_0$, $U' = U'' \equiv 0$, $V \equiv V_0$, and (22a) becomes

$$\zeta'' + V_0 \zeta' + (k^2 - kU_0)\zeta = 0, \qquad (23)$$

and is decoupled from (22b). Therefore, one may study separately the potential disturbances,

$$\zeta \equiv 0; \quad \Phi = B_m \sin{(m\phi - \phi_0)}.$$

Then, it follows from (22b) that

$$\lambda_1(m) = -m; \quad \lambda_2(m) = m.$$

This result does not depend on the U_0, V_0 values. For physical reasons the eigenvalues λ_2 and their eigenmodes are irrelevant for the outer problem $r > r_0$. Indeed, they suggest a growth of disturbances with $r \to \infty$, independent of the base flow strength. Now, one may study vortex disturbances of the form

$$\zeta = D_m \sin{(m\phi - \phi_0)}.$$

It follows from (23) that

$$\left.\begin{aligned}
\lambda_3 &= 2 + \tfrac{1}{2}U_0 - (\tfrac{1}{4}U_0^2 + m^2 + imV_0)^{\frac{1}{2}}, \\
\lambda_4 &= 2 + \tfrac{1}{2}U_0 + (\tfrac{1}{4}U_0^2 + m^2 + imV_0)^{\frac{1}{2}}.
\end{aligned}\right\} \qquad (24)$$

In particular, when U_0 is negative, but $|U_0| \gg 1$,

$$\lambda_3 = 2 - |U_0| - (m^2 + imV_0)|U_0|^{-1} + O(|U_0|^{-2}),$$
$$\lambda_4 = 2 + (m^2 + imV_0)|U_0|^{-1} + O(|U_0|^{-2}).$$

It seems that a sink flow with a large enough flow rate should be stable because the convergent flow prevents the propagation of disturbances from $r = r_0$ to infinity. Therefore we identify eigenvalues $\lambda_4(m)$ and their modes as irrelevant, because the real part of λ_4 increases without bound as m increases. It is sufficient to use only modes corresponding to $\lambda_1(m)$ and $\lambda_3(m)$ for the formation of arbitrary distributions of velocities v_r, v_ϕ, or stream function and vorticity fields (at some r), using the Fourier decomposition

$$\psi_1 = \sum_{m=1}^{\infty} [B_m r^{-m} + (\lambda^2 - m^2) r^\lambda D_m] \sin{(m\phi - \phi_0)},$$

where $\lambda = \lambda_3(m)$. The constants B_m and D_m are to be determined for the flow specified at $r = r_0$. The term with $m = 0$ is absent because we consider disturbances having zero flow rate. As $\lambda_1(m) = -m$ does not depend on parameter values, it is sufficient to examine only λ to study stability. We saw that $\lambda_r < 0$ for $U_0 \ll -1$. Instability appears when λ_r passes through zero as U_0 increases. In the neutral case λ is purely imaginary; say, $\lambda = -im\beta$, where β is real. Then we produce the known dispersion relations (8)–(10). Note that $\lambda_r < 2$ at all bounded values of U_0 and V_0, as is evident from (24). This means that vorticity ω, being proportional to $r^{-2}\Omega_1$ (and $\Omega_1 \sim \exp{(\lambda\xi)} \sim r^{\lambda r}$), does not increase as $r \to \infty$, contrary to the behaviour of the stream function ψ_1 (which is $\sim r^{\lambda r}$).

If V_0 is fixed and U_0 is increased starting from a negative value, so that the sink becomes weaker, the exponents λ subsequently change the sign of their real parts at the neutral curves (10). Note that swirl is a stabilizing factor in that instability starts at a higher U_0, as V_0 is increased (figure 4). The first change occurs for $m = 1$. With $U_0 \to \infty$, we get from (24) that

$$\lambda = 2 - (m^2 + im V_0)/U_0 + O(U_0^{-2}).$$

The number of harmonics whose amplitudes increase as $r \to \infty$ becomes larger when U_0 grows. To predict the type of flow that develops for $r \gg r_0$, nonlinear theory must be used. It is possible that the flow tends to a non-uniform self-similar solution. To check this possibility we need to study the spatial stability of these solutions (discussed next).

4.3. *Stability of the secondary flows in free space*

Typically, the development of disturbances of non-uniform solutions must be studied numerically; but our analytical approach may be successful near bifurcation points. We have found that the vortex source is stable to infinitesimal steady disturbances when U_0, V_0 correspond to the region to the left of curve $m = 1$ in figure 4. We also know that the bifurcations of the secondary solutions are subcritical with respect to U_0. The general theory states that in such a case the secondary solutions are unstable in the vicinity of a bifurcation point, if non-degenerate. The following analysis confirms this but provides some new information on the values of λ_r, on neutral disturbances and on resonance cases. To avoid bulky calculations we shall focus on the relatively simple case $V_0 = 0$ (figure 5). Owing to continuation arguments the main results would be the same in weakly swirling flows.

Thus we use (22) with $V = 0$ and from §3.2, we get

$$U = U_0 + A u_1 + A^2 u_2 + \ldots = U_{0*} + A \cos(m\phi) + A^2(u_2 - 1/(12 m^2)) + \ldots$$

or

$$U = \frac{m^2 - 4}{2} + A \cos(m\phi) - \frac{A^2}{12 m^2}[1 + 2 \cos(m\phi) - 2 \cos(2m\phi)] + O(A^3),$$

and solutions are constructed with the help of the expansions,

$$\zeta = \zeta_0 + A\zeta_1 + A^2\zeta_2 + \ldots; \quad \Phi = \Phi_0 + A\Phi_1 + A^2\Phi_2 + \ldots; \quad k = k_0 + Ak_1 + A^2k_2 + \ldots.$$

At the zeroth order of A,

$$\zeta_0'' + [k_0^2 - \tfrac{1}{2}k_0(m^2 - 4)]\zeta_0 = 0.$$

The requirement of periodicity of ζ_0 yields

$$k_0^2 - \tfrac{1}{2}k_0(m^2 - 4) = n^2, \quad n = 1, 2, \ldots.$$

Thence,

$$k_0 = \tfrac{1}{4}\{m^2 - 4 - [(m^2 - 4)^2 + 16 n^2]^{\frac{1}{2}}\};$$

$$\zeta_0 = \cos(n\phi - \phi_0).$$

From (22),

$$(\lambda^2 - n^2)\Phi_0 = \cos(n\phi - \phi_0).$$

The minus sign before the radical in the expression for k_0 is chosen for the same reason as in §4.2. For the particular case, when $n = 1$, $m = 2$ (note that this is the subharmonic resonance case), we get $k_0 = -1$ and $\lambda = 1$. Hence the last equation has no solution, and an alternative approach is needed. But in non-resonance cases,

$$\Phi_0 = \frac{\cos(n\phi - \phi_0)}{\lambda^2 - n^2}.$$

If $m > 1$, the solutions are not stable because a set of eigenvalues for the non-uniform solution is close to the one for the uniform flow at $A \ll 1$, and the uniform solution is unstable. Therefore, resonance takes place in the region of instability of both the base and the secondary solutions. To check the instability of the secondary solutions in the subcritical vicinity of the main neutral curve, we have to study only the case $m = 1$, $n = 1$. For these parameter values, using the decomposition for ζ above, (22) and the solvability conditions, we get

$$k_0 = -2, \lambda_0 = 0, \quad \zeta_0 = \cos{(\phi - \phi_0)}, \quad \Phi_0 = -\cos{(\phi - \phi_0)};$$

$$k_1 = \lambda_1 = 0, \quad \zeta_1 = \tfrac{2}{3}\cos{(2\phi - \phi_0)}, \quad \Phi_1 = -\tfrac{1}{6}\cos{(2\phi - \phi_0)}.$$

From solvability conditions for the second-order equations,

$$k_2 \cos{\phi_0} = 0; \quad (\tfrac{5}{2}k_2 - \tfrac{1}{3})\sin{\phi_0} = 0.$$

There are two possibilities:

Case (a): $\phi_0 = 0$; $k_2 = 0$.

In this case all $k_i = 0$; $i = 1, 2, \dots$. The disturbance is neutral ($\lambda = 0$) and denotes a turn in the velocity field around the origin. It has already become evident that the secondary solutions permit such a transformation.

Case (b): $\phi_0 = \tfrac{1}{2}\pi$; $k_2 = 2/15$; $\lambda = 2/15A^2 + O(A^4)$.

This disturbance is amplifying, and therefore, in accordance with the general theory, the secondary regime is unstable. Our numerical calculations have shown that the secondary regime with $m = 1$ remains unstable also at large amplitudes. Thus, only the uniform sink flow for $Re < -3\pi$ is found to be stable to the perturbations considered. In any source flow, disturbances grow downstream and the flow cannot tend to one of the secondary solutions as $r \to \infty$. This result together with the general theory suggests that all secondary swirling flows are also unstable. They possess similar neutral disturbances corresponding to a turn around the origin. For continuation reasons the subharmonic resonance happens in the swirling case also. This resonance is meaningful in a study of nonlinear development of disturbances in the supercritical region. Although the secondary solutions are unstable, transition trajectories connecting them with the base solution may be stable in the subcritical region and are of physical interest. For approximate studies of such trajectories, we need eigenvalues for the primary and secondary solutions. In the next section we calculate such eigenvalues for the JH problem.

4.4. *Spatial stability of the JH flow*

This topic has been studied in prior papers in some detail (see Banks *et al.* 1988), but we need some additional information before we can study the reattachment phenomenon (discussed later). Furthermore, we shall see that in contrast to the vortex-source case, here the relevant and irrelevant modes mix in an unstable region where their eigenvalues become complex. In our calculations we use the following numerical algorithm. The system (22) with $V \equiv 0$ is integrated from $\phi = 0$ to $\phi = \alpha$ using the initial conditions,

$$\Phi(0) = \Phi'(0) = 0; \quad \zeta(0) = 1; \quad \zeta'(0) = B.$$

The first two are no-slip conditions, the third is a normalization condition and B is a number to be chosen to satisfy $\Phi'(\alpha) = 0$. As the problem is linear, the value of
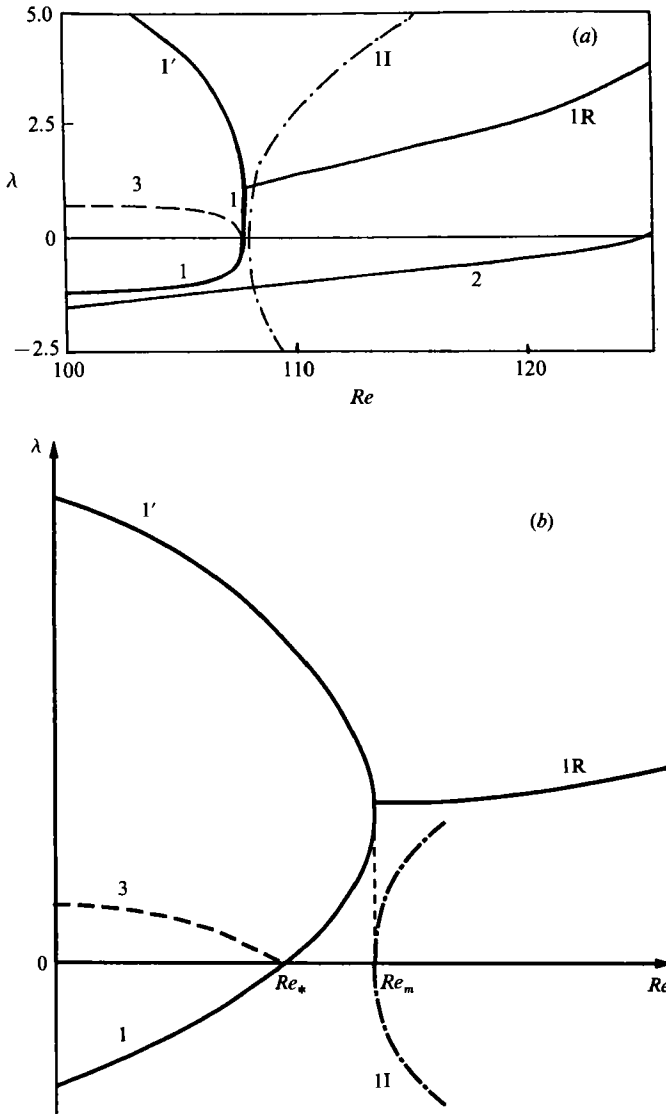
FIGURE 13. (a) Eigenvalues for the JH flow at $\alpha = 10°$. Curves 1R and 1I correspond to real and imaginary parts of λ; the other curves correspond to real λ. The main relevant $(1, 2)$ and irrelevant $(1')$ eigenvalues of solutions O $(Re < Re_*)$ and OIO $(Re > Re_*)$, and the main eigenvalue of solution IO (3) are shown. (b) A schematic of an enlarged region near Re_* and Re_m.

B is unique and is found with the help of the shooting method. Then we examine $\Phi(\alpha)$ as a function of λ and look for zeros of this function. In all our calculations, we have used the fourth-order Runge–Kutta integration procedure and a fixed non-uniform (Chebyshev) grid with 100 intervals. The results have been checked against analytical solutions and numerical results of other authors in a few cases.

Calculated results for a divergent channel with $\alpha = 10°$ are shown in figure 13(a). The solid curves correspond to λ_r values for the everywhere-divergent solution O at $Re < Re_*$ and for solution IOI at $Re > Re_*$ (figure 1). The critical value $Re = Re_* = 108$, at which λ (1), being real, changes its sign, corresponds to the point B_1 in figure 1. In accordance with prior results (e.g. Banks *et al.*) and for physical reasons, we
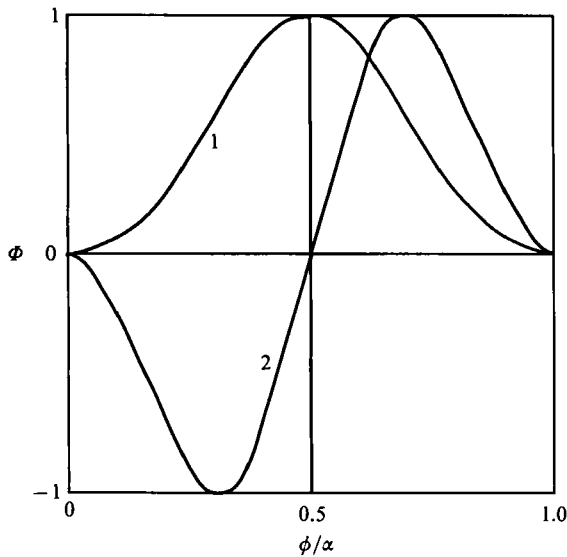
FIGURE 14. Eigenfunctions of neutral disturbances of symmetric and antisymmetric modes 1 and 2 (for points B_1 and M_1 in figure 1).

suppose that at $Re = 0$ the solution O is stable, and we identify relevant ($\lambda_r < 0$) and irrelevant ($\lambda_r > 0$) modes. In figure 13 relevant modes pertain to curves 1 and 2, and one of the irrelevant modes is denoted by curve $1'$. At $Re = Re_m$ which is slightly larger than Re_*, the eigenvalues corresponding to curves 1 and $1'$ merge, and the complex-conjugate pair appears with real and imaginary parts corresponding to curves 1R and 1I (dot-dashed). This is elucidated with an expanded sketch in figure 13(b). We see that the relevant and irrelevant modes become mixed after the merging. The second mode (curve 2), belonging to solution O for $Re < Re_*$ and to solution IOI for $Re > Re_*$, turns to zero at $Re = 124$ which corresponds to the bifurcation point M_1 in figure 1. The dashed curve 3 in figure 13(a) denotes the main eigenvalues of solution IO (or OI). This mode is considered to be relevant for continuation reasons. Solutions O and IO coincide at $Re = Re_*$, as do their eigenvalues. As one moves along curve O to point B_1 and then along IO in figure 1, one also moves from curve 1 to curve 3 in figure 13.

The mode represented by curve 3 in figure 13 will be used in the analysis of the reattachment phenomenon given below. Eigenfunctions $\Phi(\phi)$, related to curves 1 and 2 in figure 13, are shown in figure 14 for the parameter values corresponding to points B_1 and M_1 in figure 1.

The appearance of the complex-valued λ in the supercritical range of Re together with instability of all the JH solutions suggests the existence of solutions which are either periodic or chaotic with respect to $\xi = \ln(r/r_0)$. The search for such solutions is rather difficult and requires a separate study.

4.5. *Spatial stability of time-dependent disturbances*

Analysis of time-dependent disturbances is rather complicated for the JH solutions and the secondary regimes in free space, because coefficients of equations for the disturbances depend on both r and ϕ. But in the case of the vortex-source flow, the base velocity field depends only on r, a fact that allows us to reduce the linear stability problem to an ordinary differential equation. here we consider the stability

of the source flow. Starting from equations (1) with $v_r = \nu U_0/r$, $v_\phi = 0$ for the base flow, we obtain the linearized equation for disturbance vorticity

$$\frac{\partial\omega}{\partial\tau} + \frac{U_0}{r}\frac{\partial\omega}{\partial r} = \frac{1}{r}\frac{\partial}{\partial r}\left(r\frac{\partial\omega}{\partial r}\right) + \frac{1}{r^2}\frac{\partial^2\omega}{\partial\phi^2}.$$

Because the base flow is potential, here we use ω for disturbance vorticity; $\tau = \nu t/r_0^2$, and r is normalized by r_0. Then disturbances may be sought in the normal form $\omega = f(r)\exp(\gamma\tau + im\phi)$, and $f(r)$ must satisfy the equation

$$r^2\frac{\mathrm{d}^2 f}{\mathrm{d}r^2} + r(1 - U_0)\frac{\mathrm{d}f}{\mathrm{d}r} - (\gamma r^2 + m^2)f = 0. \tag{25}$$

The solutions of (25) are explicitly written in terms of Bessel functions. To select a 'relevant' mode we use the condition that at $\gamma = 0$ the solution must coincide with

$$f = \left(\frac{r}{r_0}\right)^k, \quad k = \tfrac{1}{2}U_0 - (\tfrac{1}{4}U_0^2 + m^2)^{\frac{1}{2}},$$

corresponding to the steady case studied in §4.2.

This yields $\qquad f = r^p H_q^{(2)}(r(-\gamma)^{\frac{1}{2}}); \quad p = \tfrac{1}{2}U_0; \quad q = (\tfrac{1}{4}U_0^2 + m^2)^{\frac{1}{2}}.$

Here, $H_q^{(2)}$ is the Hankel function. Let, at $r = 1$, there is harmonic oscillating disturbances which propagate to the outer region. In this case $\gamma = i\kappa$, with real κ being a frequency. Using the asymptotic expression for the Hankel function (Abramowitz & Stegun 1964, p. 364), we obtain

$$f = C r^{p-\frac{1}{2}}\exp(-r\pi\tfrac{1}{4}\kappa)^{\frac{1}{2}} + \dots; \quad \kappa > 0.$$

One may see that at non-zero frequency we have exponential decay of the disturbances at infinity. Therefore, the steady disturbances, corresponding to zero frequency, are the most dangerous.

4.6. *Behaviour of temporal disturbances near the bifurcation points*

Now we consider the following boundary-value problem of a flow in the region $r_0 < r < r_1$. On the boundaries we formulate 'soft' conditions which are satisfied for all the self-similar solutions considered. Namely, we suppose that

$$\frac{\partial\Psi}{\partial r} = 0; \quad \frac{\partial\Omega}{\partial r} = 0 \quad \text{at} \quad r = r_0 \text{ and } r = r_1.$$

Then we consider time-dependent disturbances which must satisfy the same boundary conditions. Using the variable $\zeta = \ln(r/r_0)$ and the transformation $w = r^2 f$, we obtain from (25)

$$\left.\begin{aligned}
\frac{\mathrm{d}^2 w}{\mathrm{d}\xi^2} - (U_0 + 4)\frac{\mathrm{d}w}{\mathrm{d}\xi} + (4 - m^2 + 2U_0)w &= \gamma w\exp(2\xi); \\
\frac{\mathrm{d}w}{\mathrm{d}\xi} = 0 \quad \text{at} \quad \zeta = 0 \text{ and } \xi = \xi_1 = \ln\frac{r_1}{r_0}, \quad w(0) &= 1.
\end{aligned}\right\} \tag{26}$$

The last condition is a normalization which may be used without any loss of generality in this linear problem. It is obvious that at $U_0 = U_{0*} = \tfrac{1}{2}(m^2 - 4)$, there is a 'neutral' solution $\gamma = 0$, $w \equiv 1$.

We should like to know if $\gamma(U_0)$ becomes positive for $U_0 > U_{0*}$. For this we have to calculate the derivative $\mathrm{d}\gamma/\mathrm{d}U_0$. The eigenvalue γ and the eigenfunction w of (26) have smooth dependence on U_0, and we use the expansions

$$U_0 = U_{0*} + \epsilon; \quad \gamma = \epsilon\gamma_1 + \epsilon^2\gamma_2 + \dots; \quad w = 1 + \epsilon w_1 + \dots.$$

At the zeroth order we have an identity. At the first order, it follows from (26) that

$$\frac{\mathrm{d}^2 w_1}{\mathrm{d}\xi^2} - (U_{0*} + 4)\frac{\mathrm{d}w_1}{\mathrm{d}\xi} = \gamma_1 \exp(2\xi) - 2.$$

Integration yields

$$\frac{\mathrm{d}w_1}{\mathrm{d}\xi} = C \exp\{(U_{0*} + 4)\xi\} + \frac{2}{U_{0*} + 4} - \frac{\gamma_1}{2(U_{0*} + 2)} \exp(2\xi).$$

Using the boundary conditions in (26) and eliminating the integration constant C we obtain

$$\gamma_1 = 4\frac{U_{0*} + 2}{U_{0*} + 4}\frac{1 - \exp\{-(U_{0*} + 4)\xi_1\}}{1 - \exp\{-(U_{0*} + 2)\xi_1\}}.$$

Because $U_{0*} > -1.5$, γ is proportional to ϵ with a positive multiplier. This is true for arbitrary ξ_1 and, in particular, for $\xi_1 \to \infty$.

Therefore, the temporal instability happens together with the spatial instability, and growing modes are monotonic in time near the neutral curves.

5. Transition trajectories

The stability analysis shows that all secondary solutions are unstable both in channel flows and the free-space problems. The base solutions are unstable at supercritical Re values; they are stable to infinitesimal steady disturbances for $Re < Re_*$. But in this case, the base solutions are not global attractors because a countable set of other steady solutions exists. Here we shall study some transition trajectories which connect the spatially unstable secondary solutions to the base solutions. These seem to be stable and have interesting physical interpretations.

5.1. *Jet in the sink flow*

5.1.1 *The Landau equation*

To study transition trajectories which are new steady solutions of the Navier–Stokes equation, we use the classical weakly nonlinear theory describing disturbance behaviour in the vicinity of a bifurcation point. We shall deal with the Landau equation (Landau 1944). Banks *et al.* (1988) derived and discussed the Landau equation for flow in divergent channels with walls which are planar or have small curvature, but here we apply this equation and its modifications to a number of specific flows. We start with the case which may be solved analytically, namely, the vicinity of the first bifurcation in the sink flow. It has been shown that a sink with a large enough flow rate is stable to small steady disturbances introduced at $r = r_0$. For $m = 1$ and $V_0 = 0$, it follows from (10) that $U_{0*} = -1.5$. A small parameter ϵ is introduced: $U_0 = U_{0*} - \epsilon^2 = -1.5 - \epsilon^2$, and a disturbance is sought with the help of the expansions,

$$\Omega_1(\phi, \xi) = \epsilon A(\eta)\zeta_0(\phi) + \epsilon^2 A_1(\eta)\zeta_1(\phi) + \dots,$$

$$\psi_1(\phi, \xi) = \epsilon B(\eta)\Phi_0(\phi) + \epsilon^2 B_1(\eta)\Phi_1(\phi) + \dots,$$

where $\eta = \epsilon^2 \xi$. Starting with $(7a, b)$ and retaining only terms of the order $\leqslant \epsilon^3$, we reduce them to the simpler form

$$\frac{\partial^2 \Omega_1}{\partial \phi^2} + \Omega_1 = \frac{5}{2}\frac{\partial \Omega_1}{\partial \xi} + 2\epsilon^2 \Omega_1 - 2\frac{\partial \psi_1}{\partial \phi}\Omega_1; \quad \frac{\partial^2 \psi_1}{\partial \phi^2} = \Omega_1.$$

Then using the expansions in these equations we obtain $B = A, B_1 = A_1, \dots$ and

$$\xi_0 = \cos\phi; \quad \Phi_0 = -\cos\phi;$$
$$A_1 = A^2; \quad \zeta_1 = \tfrac{1}{3}\sin(2\phi); \quad \Phi_1 = -\tfrac{1}{12}\sin(2\phi);$$
$$A_3(\zeta_2'' + \zeta_2) = \left[\frac{5}{2}\frac{\mathrm{d}A}{\mathrm{d}\eta} + 2A - \frac{1}{6}A^3\right]\cos\phi + \tfrac{1}{2}A^3\cos(3\phi).$$

From the solvability condition, the coefficient of $\cos\phi$ must be zero and we produce the Landau equation in the particular form

$$\frac{\mathrm{d}A}{\mathrm{d}\eta} = -\tfrac{4}{5}A + \tfrac{1}{15}A^3,$$

with solution $\qquad\qquad A = \{12/[1 + c\exp(8\eta/5)]\}^{\frac{1}{2}},$

where $\qquad\qquad\qquad c = 12/A_0^2 - 1; \quad A_0 = A(0).$

We see that if $A_0^2 < 12$, then $A \to 0$ as $\eta \to \infty$. But if $A_0^2 > 12$, then A becomes infinite at a finite η value. From the above solution for A, it follows that this critical value of η is $\tfrac{5}{8}\ln(-1/c)$, but as $A \to \infty$ the solution ceases to be valid. Thus, the steady solution $A = \sqrt{12}$, corresponding to the non-uniform solution of mode $m = 1$, belongs to the separatrix of the attraction region of the uniform sink solution.

Using ψ_1 above, the velocity field for the transition trajectory is obtained as follows:

$$U = U_0 + [12(U_{0*} - U_0)]^{\frac{1}{2}}\sin\phi\{1 + c\exp(8\eta/5)\}^{-\frac{1}{2}};$$

$$V = \frac{8c}{5}\sqrt{12}\,(U_{0*} - U_0)^{\frac{3}{2}}\exp(8\eta/5)[1 + c\exp(8\eta/5)]^{-\frac{3}{2}}\cos\phi;$$

where $\qquad\qquad\qquad \eta = (U_{0*} - U_0)\ln(r/r_0).$

The azimuthal velocity is a compact function localized near some r value, and the radial velocity changes from the non-uniform distribution near $r = r_0$ to the uniform as $r \to \infty$. This transition solution depends on two parameters: r_0 and A_0, which correspond to a shift along the η-axis and the choice of an initial point on the curve $A(\eta)$.

5.1.2. *Modified Landau equation*

The Landau equation, $\mathrm{d}A/\mathrm{d}\eta = \gamma A + \delta A^3$, will now be modified and used for obtaining approximate solutions in a quite wide Reynolds-number range. For transition trajectories, the following one-mode approximation will be used:

$$\psi = \psi_b + A(\xi)(\psi_s - \psi_b), \tag{27}$$

where ψ_b is a stream function of the base solution, and ψ_s is a stream function of the secondary solution. The amplitude A is normalized here by $(-\gamma/\delta)^{\frac{1}{2}}$ and has the limits

$$\lim_{\xi \to -\infty} A(\xi) = 1; \quad \lim_{\xi \to \infty} A(\xi) = 0.$$

The Landau equation then takes the normalized form

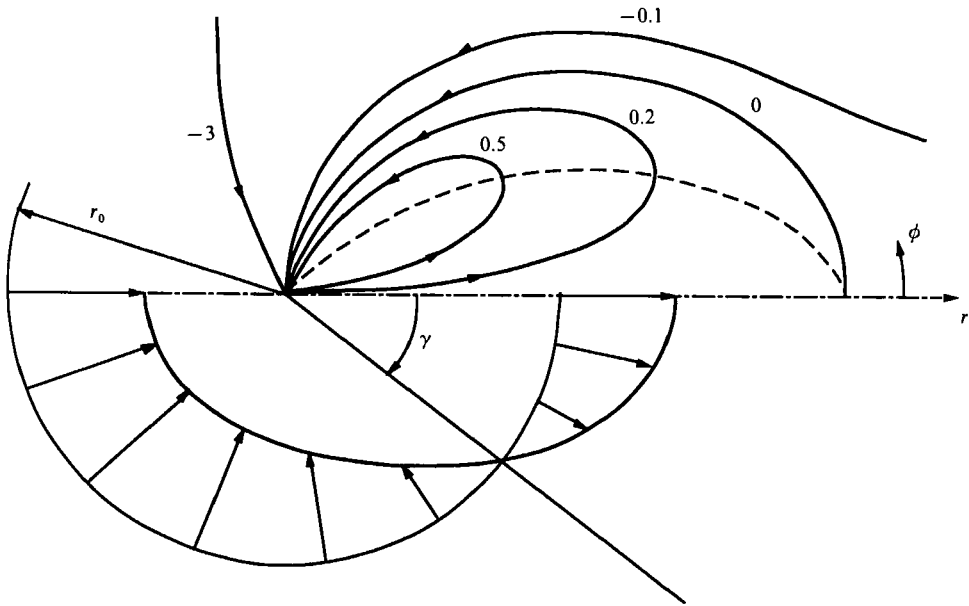$$\mathrm{d}A/\mathrm{d}\xi = \lambda A(1 - A^2), \tag{28}$$

FIGURE 15. Streamlines (top) and radial velocity distribution near the origin (bottom) for a jet in a sink flow. $U_0 = -2.615$, $V_0 = 0$, $\mu = 1$, $\lambda = -0.95$. Stream-function values are indicated.

where $\lambda < 0$ is the decay rate of such a disturbance near the base solution ψ_b in a subcritical range of the Reynolds number. The equation has the fixed point $A = 1$, besides $A = 0$, and introducing $B = 1 - A$ and $|B| \ll 1$ it follows that

$$dB/d\xi = -2\lambda B = \mu B. \tag{29}$$

As we shall see, the one-mode representation (27) is a satisfactory approximation for a quite wide range of the parameters. But the relation $\mu = -2\lambda$ is valid only in a very small neighbourhood of a bifurcation point. In order to obtain an improved approximation, we modify (28) to the form

$$\begin{aligned} dA/d\xi &= \lambda A(1 - A^2)(1 + \delta A^2), \\ \delta &= -1 - \lambda/(2\mu). \end{aligned} \tag{30}$$

Now the values of λ and μ are considered to be independent and must be found with the help of stability analysis of both the base and the secondary solutions. Equation (30) has the solution

$$r/r_0 = cA^{1/\lambda}(1 - A^2)(1 + \delta A^2)^{\delta/\mu}.$$

The constant c is arbitrary, as is r_0.

The modified equation (30) may be deduced by the weakly nonlinear approach using the higher-order terms, but we preferred a different method because it provides the exact eigenvalues of the dominant modes for both the base and secondary solutions. These eigenvalues indicate that the exponents of the disturbances decay with increasing r.

Let the initial distribution of velocity correspond to a point placed slightly below the curve 1 in figure 5. Then as r increases, the point drops to the axis $\Delta U = 0$ (see arrow T_1 in figure 5). This transition trajectory corresponds to the flow induced by a point-source jet placed together with a uniform sink at the origin. The streamlines for this flow are shown in the upper part of figure 15. Each solid curve corresponds to $\psi = \text{const}$, and values of this constant are indicated. Along the dashed curve the
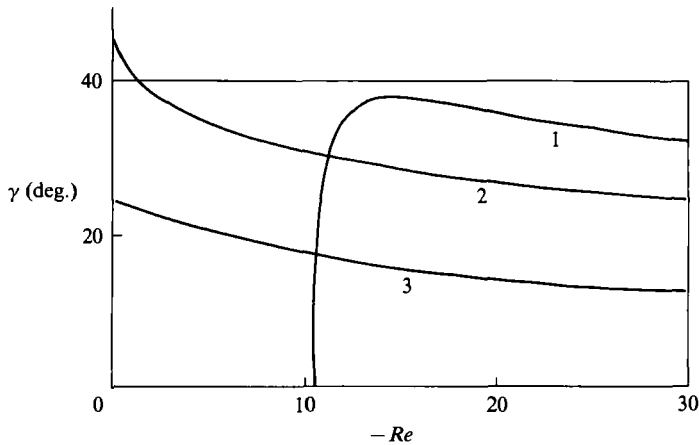
FIGURE 16. Dependence of outflow region angle on flow rate for the secondary regimes with $m = 1, 2, 3$ in sink flow.

radial velocity is zero. The lengthscale of the picture, including the curve $\psi = 0$, which is a bubble boundary, is arbitrary. This means that a trajectory T_1 (figure 5) corresponds to a family of transition solutions with r_0 being its parameter. In real flows the bubble size depends on the jet momentum.

In the lower part of figure 15, the radial velocity distribution is shown for $A = 1$, i.e. for solution 1, figure 5. There is an outflow in the sector $|\phi| < \gamma$ and inflow in the remaining sector $|\phi| > \gamma$. The half-angle γ of the outflow region depends on the flow rate, as shown by curve 1 in figure 16. Curves 2 and 3 show γ for solutions 2 and 3 in figure 5. All the curves have the common asymptote (for $Re \to -\infty$) $\gamma = 4.063 |Re|^{-\frac{1}{2}}$ as shown by asymptotic analysis in §3.2.

5.1.3. *Limitations of the weakly nonlinear approach*

It has been found that at supercritical Reynolds numbers, the steady spatial disturbances, given at some circle $r = r_0$, grow as r increases. The velocity field at large r cannot tend to one of the secondary self-similar solutions because all of them are spatially unstable. The question remains open as to what flow pattern develops at large r as a result of this instability. We will try to study this problem using some further generalizations of the Landau equation.

The simplest problem of spatial instability of the source flow will be considered. We start from the nonlinear equations for disturbances (7) with $V_0 = 0$, and simplify them using two assumptions: (i) disturbances are small; ψ_1 and $\Omega_1 \sim \epsilon, \epsilon \ll 1$ and (ii) derivatives with respect to $\xi = \ln{(r/r_0)}$ are small and $\partial/\partial \xi \sim \epsilon^2$. As we know these assumptions are indeed valid in the neighbourhood of the bifurcation points. Then, using the same approach as in §5.1.1, we reduce (7) to the system

$$(U_0 + 4)\frac{\partial \Omega_1}{\partial \xi} = \frac{\partial^2 \Omega_1}{\partial \phi^2} + (2U_0 + 4)\Omega_1 + 2\Omega_1 \frac{\partial \psi_1}{\partial \phi}; \quad \Omega_1 = \frac{\partial^2 \psi_1}{\partial \phi^2}. \tag{31}$$

Here, only terms of order $\leqslant \epsilon^3$ are retained. Other nonlinear terms, being $O(\epsilon^4)$, and the second derivatives with respect to ξ, being $O(\epsilon^5)$, are neglected. Note that all solutions of the initial system (7) which do not depend on ξ are also solutions of the reduced system (31). System (31) is valid for transition trajectories in the vicinities of the intersection points of curves 1, 2, 3 with the abscissa in figure 5. But here we

shall try to use the system in a more expanded region with large disturbances. It is obvious that system (31) is of parabolic type and allows an initial-value formulation with respect to ξ.

Calculations have been performed for a few supercritical values of $U_0 > -1.5$ and for disturbances at $r = r_0$ in the form

$$\psi_1(\phi, r_0) = A_1 \sin \phi + A_2 \sin (2\phi)$$

with some tentative values of amplitudes A_1 and A_2.

The results of the numerical calculations may be summarized as follows. With an increase in r the number of oscillations with respect to ϕ decreases and the flow pattern consists of a single region of outflow ('jet') and a rather uniform inflow in the remaining interval of ϕ. But at some value of ξ the solution becomes infinitely large. The singularity is not localized at some ϕ but is quite uniform.

It seems reasonable that the latter feature is a result of the weakly nonlinear approximation. The Landau equation (see §5.1.1), too, has similar features. Thus, this analysis shows a tendency of the solutions to consolidate into a one-jet structure, but fails to be valid for large enough amplitudes.

5.2. *Boundary-layer approximation*

The limitations of the above approximation may be avoided if one takes into account other nonlinear terms of equations (7); in the weakly nonlinear approach, these terms are of $O(\epsilon^4)$. In this case we may relax the requirement of small amplitudes in the approximation and suppose that amplitudes may be arbitrarily large but that $\partial/\partial\xi \ll \partial/\partial\phi$. Such a conjecture is usually used in the so-called 'multi-scale' approach and in the boundary-layer approximation of the Navier–Stokes equation. In numerical methods this approach is known as 'parabolization' of equations. In this case there is no reason to separate the base flow and disturbances, and we may start from equations (2) with $\partial/\partial T = 0$. Neglecting the secondary derivatives with respect to ξ, we obtain,

$$\left(\frac{\partial\psi}{\partial\phi}+4\right)\frac{\partial\Omega}{\partial\xi} = \frac{\partial^2\Omega}{\partial\phi^2}+4\Omega+2\Omega\frac{\partial\psi}{\partial\phi}+\frac{\partial\psi}{\partial\xi}\frac{\partial\Omega}{\partial\phi}; \quad \frac{\partial^2\psi}{\partial\phi^2} = \Omega. \tag{32a, b}$$

These equations, being of parabolic type, are not resolved with respect to the derivatives $\partial\Omega/\partial\xi$ and $\partial\psi/\partial\xi$; that is, if Ω and ψ are given at some $\xi = \xi_0$, then their derivatives with respect to ξ cannot be calculated explicitly from (32). But this difficulty may be overcome if we use the following semi-implicit method of integration.

We assume that at some $\xi = \xi_0$ a distribution $\psi = \psi_0(\phi)$ is known. Then from (32b) we find Ω_0 and may also calculate $\partial\Omega_0/\partial\phi$ and $\partial\psi_0/\partial\phi$. Let us introduce $z = \partial\psi/\partial\xi$ and find from (32b) that $\partial^2 z/\partial\phi^2 = \partial\Omega/\partial\xi$. Further, (32a) may be rewritten in the form

$$a\frac{\partial^2 z}{\partial\phi^2} - bz = c, \tag{33}$$

where $\qquad a = \dfrac{\partial\psi_0}{\partial\phi}+4; \quad b = \dfrac{\partial\Omega_0}{\partial\phi}; \quad c = \dfrac{\partial^2\Omega_0}{\partial\phi^2}+2\Omega_0\left(2+\dfrac{\partial\psi_0}{\partial\phi}\right).$

The next step is finding a periodic solution of (33) with period 2π. We have found the solution using factorization methods for the boundary-value problem $z(0) =$
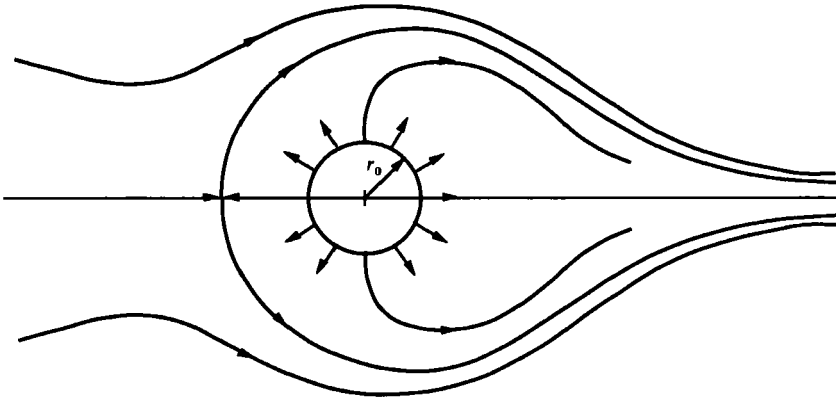
FIGURE 17. Computed streamlines for a perturbed source flow for $U_0 = 2$ calculated using the boundary-layer approximation.

$z(2\pi) = 0$. The zero value may be chosen without loss of generality because the circulation of the disturbances is zero. Finally, we find ψ_1 at the next position $\xi_1 = \xi_0 + \Delta\xi$ with the help of the relation $\psi_1 = \psi_0 + z\Delta\xi$, and perform an iteration procedure.

At $r = r_0$ we have used the same initial condition as in the previous section:

$$\psi = U_0\phi + A_1 \sin\phi + A_2 \sin(2\phi).$$

The results of calculations at small velocities are similar to the results of §5.1.3. If even $A_2 \gg A_1$ (i.e. 'two-jet' perturbation), then with an increase in r the number of oscillations in the distribution of $\psi(\phi)$ decreases and the flow tends to the one-jet pattern. Thus, the 'consolidation' effect is observed in both the approaches. But now, instead of the limitation in §5.1.3, we have another limitation.

When the minimum value of the radial velocity $U = \partial\psi/\partial\phi$ becomes less than -4, the coefficient of $\partial\Omega/\partial\xi$ in (32a) goes to zero at some values of ϕ. Though these values may lie between grid points, this leads to a fast numerical instability and destruction of solutions due to high-frequency oscillation with respect to ϕ (equation (33)). Therefore, the boundary-layer approach obviously ceases to be valid for $U_{\min} < -4$.

An example of calculations using the boundary-layer approach and parameter values $U_0 = 2$, $A_1 = A_2 = 0.1$ is shown in figure 17. We see that quasi-uniform flow at $r = r_0$ transforms into a thin jet at large r. Fluid flowing out from the source is contained in a 'bottle'-like region, outside of which we have a jet-like flow.

Thus, we see that at the first stage of flow development with increasing r, both the weakly nonlinear and boundary-layer approximations show a tendency towards flow consolidation. In the supercritical range $(Re > Re_*)$ both approaches fail to be valid at large enough r and the full Navier–Stokes equation must be used. Now we return to the weakly nonlinear approximation to describe a number of transition trajectories in the subcritical range $(Re < Re_*)$.

5.3. *Tripolar jet*

Here we consider a jet which flows out into an ambient fluid at rest. Such an example gives transition trajectory T_3 in figure 5 (with $U_0 = 0$) from the three-jet solution to the no-flow case. The initial solution, corresponding to a vicinity of the intersection point P on curve 3, is a flow containing three outflow regions and three inflow regions with maximum velocity $U_{\max} = U(0) = 22.23$ and minimum velocity $U(\frac{1}{3}\pi) = -12.44$. The velocity profile in the interval $-\frac{1}{3}\pi < \phi < 0$ is shown in the lower part of figure
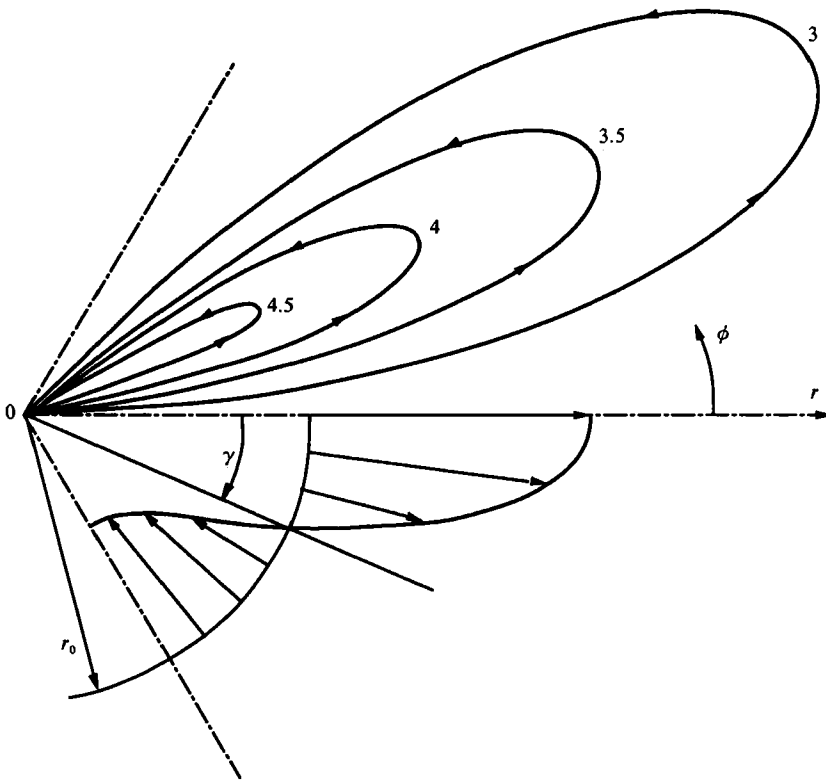
FIGURE 18. Streamlines (top) and velocity profile near the origin (bottom) for the tripolar jet in free space for zero flow rate (i.e. $U_0 = 0$). Stream-function values are indicated.

18. The rays $\phi = \frac{1}{3}k\pi$, $k = 1, \ldots, 6$ are symmetry axes. The half-angle of the outflow region $\gamma = 24.5°$. This solution (corresponding to P in figure 5) is unstable and the increment μ (equation (30)) of the growing mode $m = 3$ is 0.5456. For the uniform solution the decay rate $\lambda = \lambda_3$ is obtained from (24). In this case $U_0 = V_0 = 0$, $m = 3$, and therefore $\lambda = -1$. These provide us all the coefficients needed in equation (30) to calculate amplitude $A(\xi)$.

A few streamlines for the transition solution approximations (27) and (30) are shown in the upper part of figure 18. There is no bubble here (unlike, for example, in figure 15) and ψ is zero only along rays $\phi = \frac{1}{3}k\pi$, $k = 1, \ldots, 6$. The function $U(\phi, r)$ tends to zero as r increases and is asymptotically proportional to $1/r$ for $r/r_0 \gg 1$. Based on the results we can infer that there are three *intermediate asymptotic* regions for the tripolar jet of a high momentum and zero flow rate, namely, (*a*) the Schlichting region where the maximum velocity v_m decays in proportion to $r^{-\frac{1}{3}}$, (*b*) the JH region where v_m is proportional to $1/r$, and (*c*) the outer region where v_m is proportional to $1/r^2$.

Flow patterns similar to that shown in figure 18 have been observed in Marangoni convection (Pshenichnikov & Yatsenko 1974). At large Schmidt numbers the flow is concentrated in a thin near-surface layer and may be considered quasi-two-dimensional. When the intensity of motion increases, the number of vortices, i.e. m value, also increases, as in our case.
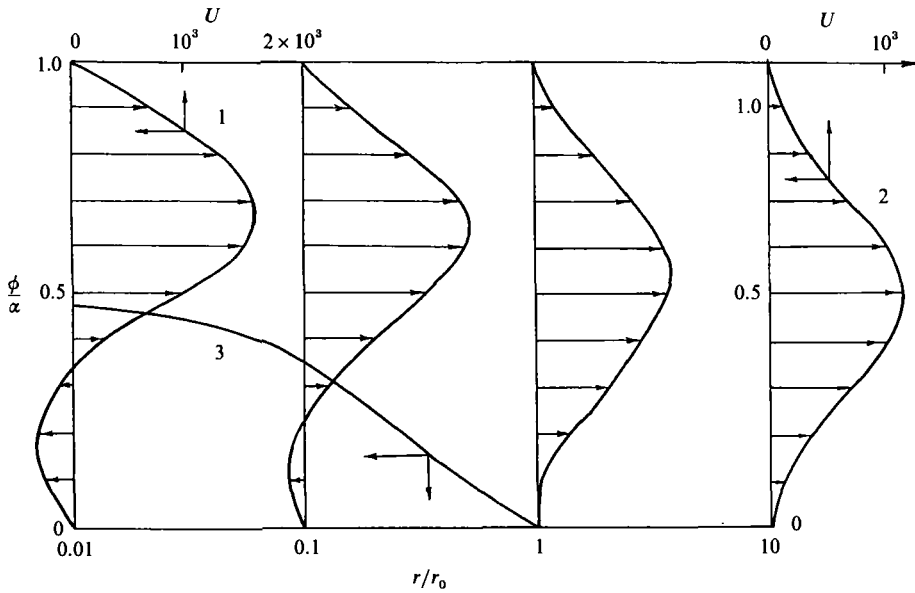
FIGURE 19. Attachment of flow in the diffuser at $Re = 100$ (transition trajectory from IO to O regimes in figure 1). Initial (curve 1), and final (curve 2) velocity distributions and boundary of the recirculation region (curve 3) are shown.

5.4. *Attachment flow in the divergent channel*

Here we consider the transition trajectory in the JH problem from solution IO to solution O at a *subcritical Re* close to Re_* (near, but below, point B_1 in figure 1). This case is simpler because we can use the weakly nonlinear theory for this study. Note that this transition implies a reattachment phenomenon as inflow disappears in the transition IO to O.

Let r_0 be the position of reattachment; for $r \ll r_0$, we consider the asymmetric self-similar solution of mode $m = 1$ with the stream function ψ_a (curve 1 in figure 19) which also contains a small disturbance $B(\psi_s - \psi_a)$; here $\psi_s(O(1))$ is the stream function of the stable symmetric solution (curve 2 in figure 19) and $0 < B \ll 1$. We look for the dependence of B on the distance r. We expect that $B \to 0$ as $r \to 0$ and $B \to 1$ as $r \to \infty$, and

$$\psi(r, \phi) = \psi_a(\phi) + B(r)[\psi_s(\phi) - \psi_a(\phi)].$$

Following the procedure of §5.1.1, the Landau equation can be deduced as

$$\mathrm{d}B/\mathrm{d}\xi = \mu B(1 - B^2).$$

Its solution $B \equiv 0$ corresponds to the asymmetric self-similar solution IO, and $B \equiv 1$ corresponds to the symmetric solution O; the disturbance growth rate $\mu > 0$ because of the instability of the asymmetric solution. The dependence $\mu(Re)$ is shown by curve 3 in figure 13. Comparing this curve with curve 1 (for λ) one can see that $\lambda \approx -2\mu$ for the range $100 \leqslant Re \leqslant Re_*$. Integrating the above equation, we have,

$$B = [1 + c \exp(-2\mu\xi)]^{-\frac{1}{2}}; \quad c = 1/[1/B_0^2 - 1]; \quad B_0 = B(0),$$

where $\xi = 0(r = r_0)$ is the position of reattachment. The form of $B(r)$ is shown in figure 20. The curve separating the regions of divergent flow and the recirculation zone is found from the relation

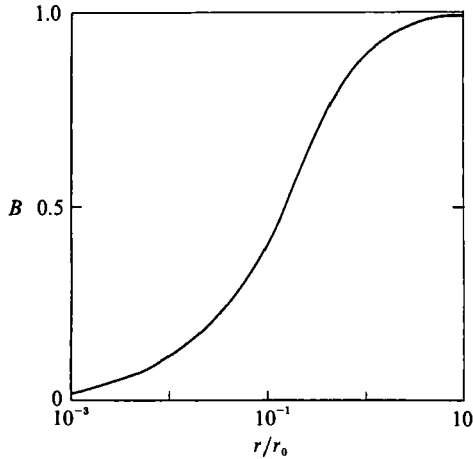$$\psi_a(\phi) + B(r)[\psi_s(\phi) - \psi_a(\phi)] = 0.$$

FIGURE 20. Dependence of the amplitude in the Landau equation on distance from the attachment point $r = r_0$; $Re = 100$; $\alpha = 10°$.
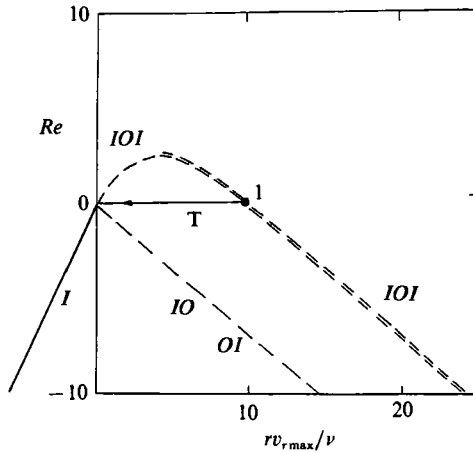

FIGURE 21. Bifurcation diagram at $\alpha = \pi$, $m = 1$. Transition trajectory (T) from regime *IOI* to the rest case (i.e. $Re = 0$). Parameters of point 1 are: $U_{max} = 11.37$, $U_{min} = -5.34$, $\gamma = 31.6°$, $\mu = 0.4756$.

This curve approaches the bottom wall at some finite angle (see curve 3 in figure 19). The angle of reattachment correspondingly decreases and approaches zero as $Re \rightarrow Re_*$. Our numerical calculations indicate that near $Re = Re_*$, the angle is proportional to $Re - Re_*$. In figure 19 the angle is near 1° (it appears larger owing to the use of the logarithmic scale for r). The attachment takes place only if $B > 0$. If an initial disturbance is of the opposite sign, then the everywhere-divergent flow will not be established, as is the case with other unstable JH solutions. The fate of the transition solution as $r \rightarrow \infty$ is unknown, but some non-self-similar flow has to develop.

5.5. *Jet emerging from a slit in a wall*

When in the JH problem the angle between the planes is π, the flow becomes a plane jet emerging from an infinitesimal thin slit in a plane wall. The dependence of Re on U_{max} for the JH solutions with $m = 1$ (which means that there is only one region of outflow) is shown in figure 21. Letters denote the same flow patterns as in figure 1. The solid curve relates to stable solutions, the dashed curves denote unstable
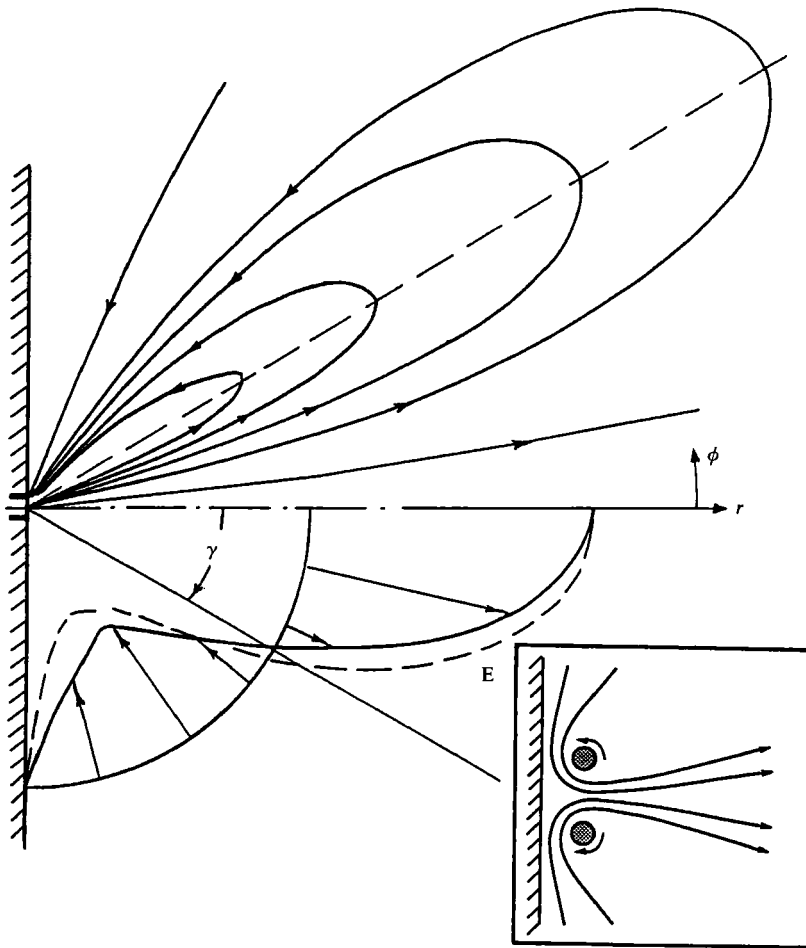
FIGURE 22. Streamlines (top) and velocity profiles (bottom) for a jet emerging from a slit in a plane wall (trajectory T in figure 21). Velocity profiles are shown for both near origin (solid line) and far region (dashed line). Insert shows a schematic of a physical realization of a jet with zero flow rate.

solutions with one growing disturbance mode, and the double-dashed curves represent unstable solutions with two growing disturbance modes. One of these modes breaks the symmetry, another retains the symmetry but causes a transition to the asymmetric solution with the smallest maximum velocity $U_{\max}$.

Now we consider such a transition for a total flow rate of zero, as this corresponds to strong jets when momentum flux is the unique characteristic of the flow (see §1). This flow may be realized experimentally with the help of two thin counter-rotating cylinders placed near a wall (see the schematic in the insert in figure 22). The rotation direction must produce an outflow near the symmetry plane and inflows near the wall. The JH solution for such a flow pattern for $Re = 0$ corresponds to point 1 in figure 21. The velocity profile is shown in the lower part of figure 22.

To approximate the transition solution T (see figure 21) we will use (27) and (30). We must determine λ and so must study the stability characteristics of the state of rest following Dean & Montagnon (1949). Looking for symmetric small disturbances of the normal form, we find

$$\psi = \exp{(\lambda\xi)}\{C_1 \sin{[(\lambda-2)\phi]} + C_2 \sin{(\lambda\phi)}\}. \tag{34}$$
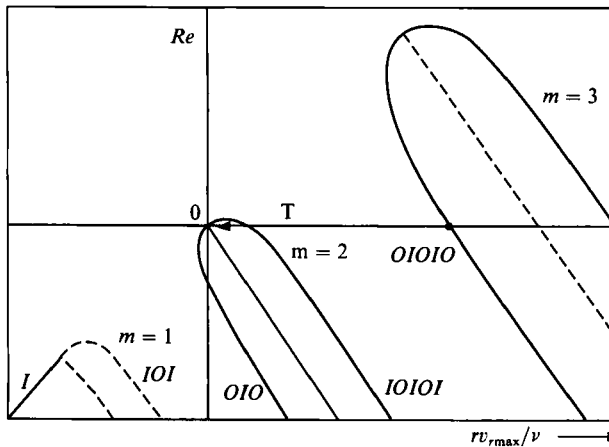
FIGURE 23. Bifurcation diagram at $\alpha = 2\pi$; $m = 1, 2, 3$. Parameters for the starting point of transition trajectory T (from *OIOIO* to 0, the rest case) are: $U_{max} = 17.24$, $U_{min} = 10.96$, $\gamma = 26.9°$, $\mu = 0.4836$.

From the conditions $\psi(\tfrac{1}{2}\pi) = \psi'(\tfrac{1}{2}\pi) = 2$ we have

$$(C_2 - C_1)\sin(\tfrac{1}{2}\lambda\pi) = 0; \quad \{\lambda C_2 - (\lambda - 2)C_1\}\cos(\tfrac{1}{2}\lambda\pi) = 0,$$

and using the normalization $\psi'(0) = 1$ we obtain

$$\lambda = -1, -3, \ldots; \quad C_1 = C_2 = 1/(2\lambda - 2);$$

$$\lambda = -2, -4, \ldots; \quad C_1 = 1/[2(\lambda - 2)]; \quad C_2 = 1/(2\lambda).$$

The minimum decay corresponds to $\lambda = -1$ and

$$\psi = \tfrac{1}{4}[\sin\phi + \sin(3\phi)]; \quad \psi' = U = \tfrac{1}{4}[\cos\phi + 3\cos(3\phi)].$$

This velocity distribution is shown by dashed curve E in figure 22. It is apparent that the profile does not vary significantly along the transition trajectory T (from *IOI* near the origin to the rest state at $r \to \infty$) in figure 21. Streamlines calculated with the help of (27) and (30) are shown in the upper part of figure 22. The intermediate asymptotes in this case are the same as for the tripolar jet.

Thus, employing quite a simple analysis, we have obtained a complete solution for the jet flow. It follows from $\lambda = -1$ and (34) that the stream function is proportional to r^{-1}. Physically the result obtained means that owing to interaction with the wall, the jet decays more rapidly. Near the slit the velocity decays as r^{-1} but in the far field as r^{-2}.

5.6. *Jet emerging from a thin plane channel*

One more physically interesting case is when the angle between the walls is 2π. Both walls are placed at $\phi = \pi$ and constitute a plane channel with an infinitesimal gap through which a jet emerges. This is equivalent to two counter-rotating needles near the edge of a thin plate (shown schematically as the insert in figure 24). The difference between this flow and the tripolar jet in free space is that now the no-slip condition must be satisfied at $\phi = \pm\pi$. Re (U_{max}) for the JH solutions of modes $m = 1, 2, 3$ is shown in figure 23. Again, we shall consider the transition solution with zero flow rate. The first JH solution corresponding to outflow near the axis ($\phi = 0$) has a flow
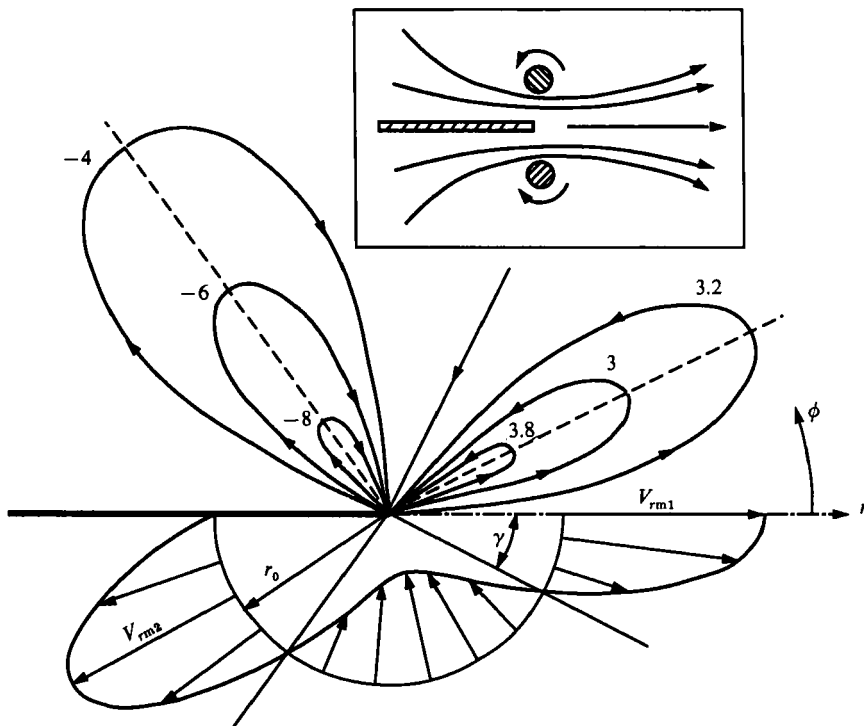
FIGURE 24. Streamlines (top) and velocity profile (bottom) for a jet emerging from a plane channel (trajectory T in figure 23). Insert shows a schematic of a physical realization.

pattern *OIOIO*. The velocity distribution is shown in the lower part of figure 24. To find λ, we have to use (34) and the conditions $\psi(\pi) = \psi'(\pi) = 0$, which yield

$$(C_1 + C_2) \sin(\lambda\pi) = 0; \quad [(\lambda C_2 + (\lambda - 2) C_1] \cos(\lambda\pi) = 0.$$

The normalization condition $\psi'(0) = 1$ gives $\lambda C_2 + (\lambda - 2)C_1 = 1$; therefore $\lambda = -\frac{1}{2}$, $-\frac{3}{2}, \dots; C_2 = C_1 = \frac{1}{2}$. The least-decaying disturbance corresponds to $\lambda = -\frac{1}{2}$ and

$$\psi = \tfrac{1}{2}[\sin(\tfrac{5}{2}\phi) - \sin(\tfrac{1}{2}\phi)]; \quad U = \tfrac{1}{4}[5\cos(\tfrac{5}{2}\phi) - \cos(\tfrac{1}{2}\phi)].$$

A streamline pattern, produced with the help of (27) and (30), is shown in the upper part of figure 24. Such a flow structure, including four vortex cells, may be interpreted as follows. The main jet propagating along the axis $\phi = 0$ entrains ambient fluid and hence induces a transverse convergent flow in the outer region. A part of this convergent flow is reflected by the wall and generates two reverse near-wall jets. A self-similar solution for the near-wall jet in the boundary-layer approximation has been reported by Akatnov (1953) and Glauert (1956); see also Loitsyansky (1966). The maximum velocity, V_{rm2} (figure 24), of this jet is proportional to $r^{-\frac{1}{2}}$. Thus, there are three asymptotic zones. In the outer region, velocity decays as $r^{-\frac{3}{2}}$ in all directions; in the intermediate JH region velocity decays in all directions as $1/r$; but in the inner region where boundary layers are present, the maximum velocity of the forward (Schlichting) jet is proportional to $r^{-\frac{1}{3}}$ and the maximum velocity of the induced near-wall Akatnov–Glauert jet is proportional to $r^{-\frac{1}{2}}$. Both jets are of the same order in the JH region but as $r \to 0$ the Schlichting jet obviously predominates.

6. Discussion

6.1. *What results from instability?*

We have found a countable set of steady flow plane solutions of the Navier–Stokes equation which bifurcate from the potential vortex-source flow. Next we studied their linear and nonlinear instabilities in the region $r > r_0$. The base solution is unstable at the flow rate and circulation values corresponding to the right-hand side of the curve $m = 1$ in figure 4. All the secondary solutions are unstable as well. This situation is similar to the JH problem whose stability features have been studied and discussed by Banks *et al.* (1988) and re-examined here for some specific values of the angle.

A mechanism for such a spatial instability seems to be rather simple. If we consider an inviscid fluid, then the instability may be explained with the help of the Bernoulli integral. If, along a radial line, velocity becomes larger than that in the ambient fluid, then pressure decreases along that line. As a result there is flow towards the low-pressure points and the velocity difference increases between this and other locations. This leads to the formation of a jet. Viscous diffusion and dissipation are stabilizing factors. This is why in the divergent channel the instability appears only if the Reynolds number exceeds some critical value. But for a large enough angle of the channel or for a source in free space, the instability develops at arbitrarily small Reynolds numbers.

One may think that this paradoxical effect (i.e. instability at $Re = 0$) occurs because of the singularity in the origin; this is not so. If a purely divergent velocity distribution is assumed at $r = r_0$ and we study the flow in the region $r > r_0$, then disturbances also increase downstream at arbitrarily small Re.

Here we consider the simplest stability problem formulation. But other approaches are possible also. For example, one may fix a velocity field at all boundaries, including at inflow and at infinity, introduce initial disturbances only at inner points of the region and then study the time evolution of the disturbances. In this case, as we have studied by numerical calculations for the free-space problem, the uniform flow (of both the source and sink) with velocity distribution fixed at $r = r_0$ is stable at all Re. In contrast, as we have shown here, infinitesimal steady disturbances at $r = r_0$ in a uniform source flow leads to the destruction downstream of the uniformity of the flow (say, by formation of jets) even when the flow rate is arbitrarily small. Such an instability is sometimes interpreted as the breakdown of St Venant's principle (see Moffatt & Duffy 1980 and Banks *et al.* 1988 for the JH problem).

To summarize, the question remains open as to what flow pattern develops at $Re > Re_*$ or at $Re < Re_*$ for large initial disturbances.

6.2. *Possible applications*

It is useful to discuss possible applications of the new solutions reported in this paper to real flows. Although our discussion here is speculative, we hope that it will serve as a motivation for further investigations.

6.2.1. *Vortex dynamics*

Steady solutions bifurcating from a potential vortex may serve as simple static models of 'elementary' events in vortex dynamics. The first example is a single vortex generated by the free-shear-layer instability. Its core seems to be similar to the core of asymmetric vortices with $m = 1$ and a high enough circulation (see, for instance, figure 9*d*). There are streamlines which swirl inward, turn and then swirl
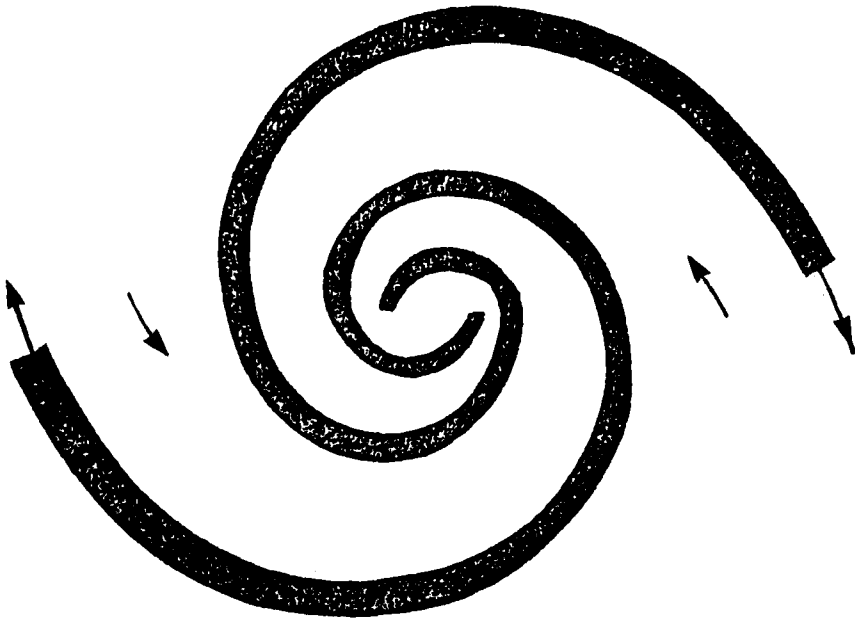
FIGURE 25. Spiral branch pattern of the nonuniform vortex-sink flow with $m = 2$. Outflow regions are darkened.

outward, so that the kinematics in our steady solution and in a free-shear-layer vortex is qualitatively same. The second example is pairing of vorticity patches. This may be modelled by the asymmetric vortices with $m = 2$ (see figure 10e) using a quasi-steady approach. Similar interactions and merging of m vortices may be modelled. The third example is vortex filamentation. Deem & Zabusky (1978) found that a vortex patch having an egg-like pattern in an inviscid fluid generates in time a vortex filament developing from the patch's edge and having a spiral form. If one takes a steady solution, like that shown in figure 9(a), as the initial distribution and removes the singularity at the origin (say, stop the rotation of a rod that drives the singularity), then a vortex patch with a spiral tail develops. Note that in our case of viscous fluid there are regions of oppose-signed vorticity that relate to the jet-like character of the flow.

6.2.2. *Spiral galaxy*

Considering a very crude idealization of a spiral galaxy we suppose that all its matter, contained in a plane, moves owing to self-gravitation and an initial angular momentum. For a viscous incompressible fluid the gravity force, being potential, may be included in the pressure gradient, and then the problem is reduced to a purely kinematic one. The simplest model is the vortex-sink flow. Even in such an extremely simplified pure kinematic model that is a mechanism of instability of the initially angle-uniform flow which leads to the generation of spiral branches (figure 25).

6.2.3. *Vortex-ring instability*

Vortex rings are typical elements of flow in round submerged jets in their near and far fields. Jet-like flows are also rich in instability phenomena including azimuthal symmetry breaking and reorganization (Hussain & Husain 1989). Vortex ring instability has been studied experimentally and theoretically by Widnall & Sullivan (1972). They have used inviscid flow to explain the instability in terms of the value
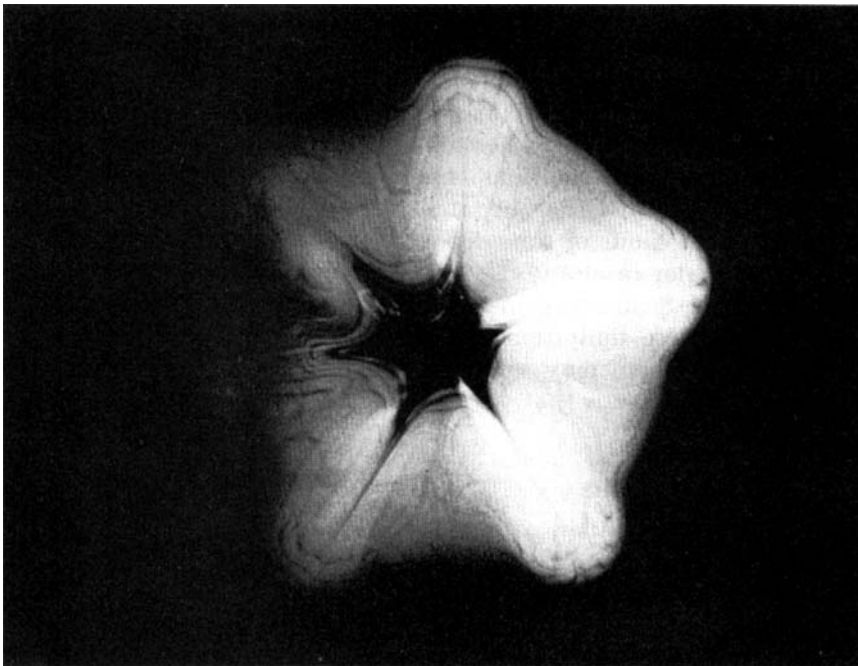
FIGURE 26. Visualization of vortex ring instability by Widnall & Sullivan (1972).

of azimuthal number m, which is related to the size of the vortex ring core. The visualized vortex ring (see figure 26) does not seem to be extremely thin, and the effect of viscosity may be significant. We shall now try to interpret this instability in terms of our results. When a fluid particle moves along a streamline in a vortex ring, its radial velocity oscillates with zero mean value. If we approximate the flow locally by the self-similar radial solutions (assuming the flows is quasi-steady), then a point in figure 5 associated with a fluid particle would oscillate near $U_0 = 0$ on the abscissa. The number m of amplifying (unstable) modes depend on the oscillation amplitude which relates to the maximum circulation in the vortex ring. According to our results, the maximum value of m is asymptotically proportional to the square root of Re (i.e. the circulation); this seems to agree with the experimental data of Widnall & Sullivan. We are surprised by this agreement as our model is crude.

6.2.4. *Near-wall eddies in plane jets*

Results of §§5.5 and 5.6 may be used as models of near-exit eddies which are observed in plane or elliptic jets (Hussain & Husain 1989). Our results are related to the far fields of these eddies. To predict the position of an eddy centre one has to combine our solution with the Schlichting boundary-layer jet solution using the method of matched asymptotic expansions, as has been done by Schneider, Zauner & Bohm (1987) for an axisymmetric jet issuing from a wall. This requires both theoretical and experimental efforts.

6.3. *Limitations of the results*

We have examined a number of exact solution of the Navier–Stokes equation, but all of them have self-similar features and include a singularity at the origin. When one tries to apply these results to real flows, some difficulties will be encountered. First, do real flows have a region where the self-similar solution may serve as a valid

approximation ? A real diffuser has an entrance at $r = r_{in}$ and an exit at $r = r_{out}$, and the r_{out}/r_{in} ratio may not be sufficient for the use of the self-similar approach for an approximation of even the base flow. Second, we have studied some bifurcations of the self-similar solutions. If one considers some boundary conditions which are different from the conditions used here, will the bifurcations disappear ? Third, we have studied only steady solutions and their stability with respect to two-dimensional disturbances. Other instabilities, relating to three-dimensional disturbances or different kinds of time-dependent disturbances may occur at smaller parameter values. Prior results of the JH problem have shown that at very small angles, the Tollmein–Schlichting instability is more dangerous (e.g. Banks *et al.* 1988). In spite of these limitations, the new solutions and the bifurcation and instabilities discussed here may serve as useful simple models. Because of their simplicity, their advantage is that they can be studied by analytical methods.

7. Summary of new results

In conclusion, we list the new results reported in this work.

It has been found analytically that a countable infinite set of bifurcations occurs in the potential vortex-source flow of a viscous incompressible fluid. As a result, new steady solutions of the Navier–Stokes equations appear.

Weakly nonlinear analysis has shown that all these bifurcations are subcritical with respect to a flow rate increase, similar to the bifurcation in the Jeffery–Hamel problem.

Features of the new solutions have been studied, including asymptotic ones at large Reynolds numbers. In particular, asymmetric vortices, being angle-dependent generalizations of the potential vortex, have asymptotically an interesting flow structure with the Golden Mean as the ratio of outflow/inflow branch widths.

Linear spatial stability with respect to steady disturbances in the region $r > r_0$ has been studied for the primary and secondary solutions. The sink flow is stable only if the flow rate is larger than the critical value; the source flow is unstable at any flow rate. It is found for the source flow that steady spatially developing disturbances are more dangerous than time-dependent ones. If the source flow becomes unstable spatially, it becomes unstable temporally too. The addition of a circulation at the origin leads to stabilization of the source flow. All the secondary solutions appear to be unstable in this formulation, similar to the JH problem.

Linear stability of the JH flow in a divergent channel of angle $\alpha = 10°$ has been studied. It has been found that in the supercritical Reynolds-number range, the main eigenvalues become complex and coupled with a mode irrelevant for $Re < Re_*$.

A number of transition trajectories connecting the secondary unstable solutions with the stable base solution have been investigated in an approximate manner for both the free-space and channel cases. In particular, a jet in a sink flow, a tripolar jet, the reattachment phenomenon in a divergent channel, a jet emerging from a slit in a wall and a jet emerging from a plane channel have been studied.

Some scaling features have been found for the secondary solutions both in the free-space and channel cases. These scaling features allow us to precisely 'count' the number of JH solutions, depending on the dimensionless maximum velocity value.

REFERENCES

ABRAMOWITZ, M. & STEGUN, A. (ed.) 1964 *Handbook of Mathematical Functions*. National Bureau of Standards. 1064 pp.

AKATNOV, N. I. 1953 Propagation of plane laminar jet near rigid wall. *Trans. Leningrad Politechnical Inst. Mashgiz.* pp. 24–31.

AREF, H. 1983 Integrable, chaotic and turbulent vortex motion in two-dimensional flows. *Ann. Rev. Fluid Mech.* **15**, 345–389.

BANKS, W. H. H., DRAZIN, P. G. & ZATURSKA, M. B. 1988 On perturbations of Jeffery–Hamel flow. *J. Fluid Mech.* **186**, 559–581.

BATCHELOR, G. K. 1967 *An Introduction to Fluid Dynamics*. Cambridge University Press. 615 pp.

BATCHELOR, G. K. & GILL, A. E. 1962 Analysis of stability of axisymmetric jets. *J. Fluid Mech.* **14**, 529–551.

DEAN, W. R. 1934 Note on the divergent flow of fluid. *Phil. Mag.* (7), **18**, 759–777.

DEAN, W. R. & MONTAGNON, P. E. 1949 On the steady motion of a viscous fluid in a corner. *Proc. Camb. Phil. Soc.* **45**, 389–394.

DEEM, G. S. & ZABUSKY, N. J. 1978 Vortex waves: stationary 'V-states', interactions, recurrence and breaking. *Phys. Rev. Lett.* **13**, 859–862.

FRAENKEL, L. E. 1962 Laminar flow in symmetrical channels with slightly curved walls. I. On the Jeffery–Hamel solutions for the flow between plane walls. *Proc. R. Soc. Lond.* A**267**, 119–138.

FRAENKEL, L. E. 1963 Laminar flow in symmetrical channels with slightly curved walls. II An asymptotic series for the stream function. *Proc. R. Soc. Lond.* A**272**, 406–428.

GEORGIOU, G. A. & EAGLES, P. M. 1985 The stability of flows in channels with small wall curvature. *J. Fluid Mech.* **159**, 259–287.

GLAUERT, M. B. 1956 The wall jet. *J. Fluid Mech.* **1**, 626–643.

GOLDSHTIK, M. A. 1990 Viscous flow paradoxes. *Ann. Rev. Fluid Mech.* **22**, 441–472.

GOLDSHTIK, M. A. & SHTERN, V. N. 1977 *Hydrodynamic Stability and Turbulence*. Novosibirsk. Nauka. 366 pp. (In Russian.)

GOLDSHTIK, M. A. & SHTERN, V. N. 1989 Loss of symmetry in viscous flow from a linear source. *Fluid Dyn.* **24**, 151–199.

GOLDSHTIK, M. A. & SHTERN, V. N. 1990 Collapse in conical viscous flows. *J. Fluid Mech.* **218**, 483–508.

HAMEL, G. 1916 Spiralförmige Bewegungen zäher Flüssigkeiten. *Jahresbericht Deutsch. Math. Verein.* **25**, 34–60.

HOOPER, A. P., DUFFY, B. R. & MOFFATT, H. K. 1982 Flow of fluid of nonuniform viscosity in converging and diverging channels. *J. Fluid Mech.* **117**, 283–304.

HUSSAIN, F. 1986 Coherent structures and turbulence. *J. Fluid Mech.* **173**, 303–356.

HUSSAIN, F. & HUSAIN, H. S. 1989 Elliptic jets. Part 1. Characteristics of unexited and exited jets. *J. Fluid Mech.* **208**, 257–320.

JEFFERY, G. B. 1915 The two-dimensional steady motion of a viscous fluid. *Phil. Mag.* (6)**29**, 455–465.

JOSEPH, D. D. 1976 *Stability of Fluid Motions*. Part 1. Springer. 638 pp.

LANDAU, L. D. 1944 On turbulence problem. *Sov. Phys. Dokl.* **44**, 339–342.

LANDAU, L. D. & LIFSHITZ, E. M. 1987 *Fluid Mechanics*. Pergamon.

LOITSYANSKY, L. G. 1966 *Mechanics of Liquids and Gas*. Pergamon.

MILLSAPS, K. & POHLHAUSEN, K. 1953 Thermal distributions in Jeffery–Hamel flows between nonparallel plane walls. *J. Aeronaut. Sci.* **20**, 187–196.

MOFFATT, H. K. & DUFFY, B. R. 1980 Local similarity solutions and their limitations. *J. Fluid Mech.* **96**, 299–313.

OSEEN, C. W. 1927 Exakte Lösungen der hydrodynamischen Differential-gleichungen. *Arkiv für Matematik, Astr. Fysik* I (14), 1–24; II (22), 1–9.

PSHENICHNIKOV, A. F. & YATSENKO, S. S. 1974 Convective diffusion from compact source of surface-active matter. *Hydrodynamics (Scientific papers of Perm University)*, No. 5, pp. 175–181. (In Russian).

ROSENHEAD, L. 1940 The steady two-dimensional radial flow of viscous fluid between two inclined plane walls. *Proc. R. Lond.* A **175**, 436–467.

SCHLICHTING, H. 1979 *Boundary-Layer Theory*. McGraw-Hill.

SCHNEIDER, W., ZAUNER, E. & BOHM, H. 1987 The recirculatory flow induced by a laminar axisymmetric jet issuing from a wall. *Trans. ASME* I: *J. Fluid Engng.* **109**, 237–241.

SOBEY, I. J. & DRAZIN, P. G. 1986 Bifurcations of two-dimensional channel flows. *J. Fluid Mech.* **171**, 263–287.

URIBE, F. J., DIAZ, E., BRAVO, A., PERALTA FABI, R. & SOTO, R. 1989 Bifurcation diagram for the Jeffery–Hamel flow. *Winter Meeting on Statistical Physical*. World Scientific.

WIDNALL, S. E. & SULLIVAN, J. P. 1972 On the stability of vortex rings. *Proc. R. Soc. Lond.* A **332**, 335–353.

YUDOVICH, V. I. 1965 Stability of steady flows of viscous incompressible fluid. *Sov. Phys. Dokl.* **10**(4), 293–295.